ARTICLE

Two *S. pombe* septation phases differ in ingression rate, septum structure, and response to F-actin loss

Mariona Ramos[1]*, Juan Carlos G. Cortés[1]*, Mamiko Sato[2], Sergio A. Rincón[1], M. Belén Moreno[1], José Ángel Clemente-Ramos[1], Masako Osumi[2,3], Pilar Pérez[1], and Juan Carlos Ribas[1]

In fission yeast, cytokinesis requires a contractile actomyosin ring (CR) coupled to membrane and septum ingression. Septation proceeds in two phases. In anaphase B, the septum ingresses slowly. During telophase, the ingression rate increases, and the CR becomes dispensable. Here, we explore the relationship between the CR and septation by analyzing septum ultrastructure, ingression, and septation proteins in cells lacking F-actin. We show that the two phases of septation correlate with septum maturation and the response of cells to F-actin removal. During the first phase, the septum is immature and, following F-actin removal, rapidly loses the Bgs1 glucan synthase from the membrane edge and fails to ingress. During the second phase, the rapidly ingressing mature septum can maintain a Bgs1 ring and septum ingression without F-actin, but ingression becomes Cdc42 and exocyst dependent. Our results provide new insights into fungal cytokinesis and reveal the dual function of CR as an essential landmark for the concentration of Bgs1 and a contractile structure that maintains septum shape and synthesis.

Introduction

Cytokinesis is the terminal step of the cell cycle that forms a barrier to divide the cell into two daughter cells. It requires co-ordinated contractile actomyosin ring (CR) constriction and plasma membrane ingression. In fungal cells, cytokinesis requires the synthesis of a special cell wall called the division septum (Cheffings et al., 2016; García Cortés et al., 2016; Pollard, 2017). This septum is a three-layered structure formed by the simultaneous synthesis of a primary septum (PS) flanked by a secondary septum (SS) on each side (Johnson et al., 1973). In the fission yeast *Schizosaccharomyces pombe*, the PS is mainly composed of linear- and branched-$\beta(1,3)$glucan, whereas the SS only contains branched-$\beta(1,3)$glucan and some $\beta(1,6)$glucan (Humbel et al., 2001). Both the PS and SS also contain $\alpha(1,3)$glucan (Cortés et al., 2012). These major polymers are synthetized by three essential glucan synthases, which localize to the plasma membrane of the division site and growing poles (Cortés et al., 2002, 2005, 2012; Liu et al., 2002). Bgs1/Cps1 forms the linear-$\beta(1,3)$glucan of the PS (Cortés et al., 2007) and is mostly localized as a ring, tightly associated with the CR, at the edge of the septum membrane during ingression (Cortés et al., 2002; Liu et al., 2002). Cooperation between Bgs1 and CR proteins is essential for CR stability and septum formation (Arasada and Pollard, 2014; Cortés

et al., 2015; Davidson et al., 2016; Sethi et al., 2016; Martín-García et al., 2018). Bgs4 forms the major cell wall polymer, branched-$\beta(1,3)$glucan, which is required for cell integrity and for coupling septum synthesis to the otherwise faster membrane ingression (Cortés et al., 2005; Martins et al., 2011; Muñoz et al., 2013). Ags1/Mok1 forms the $\alpha(1,3)$glucan, which is essential for cell integrity and is required for the PS adhesion strength needed to withstand the turgor pressure during cell separation (Hochstenbach et al., 1998; Katayama et al., 1999; Cortés et al., 2012).

It has been proposed that the fission yeast CR sets its own tension and other processes set the rate of CR constriction (Stachowiak et al., 2014). The prevailing model for cytokinesis assumes that CR constriction requires the tension developed by the interaction of myosin-II with F-actin (Wang, 2005; Eggert et al., 2006; Green et al., 2012; Glotzer, 2017). Thus, the loss of F-actin in the presence of Latrunculin A (LatA), a drug that rapidly depolymerizes F-actin and sequesters the actin monomers (Pelham and Chang, 2002; Wu et al., 2003; Proctor et al., 2012; Fujiwara et al., 2018), implies the loss of both CR tension and actomyosin-mediated contractility.

Previous examination of fission yeast cytokinesis with LatA led to the proposal that most of the force required for septum

[1]Instituto de Biología Funcional y Genómica and Departamento de Microbiología y Genética, Consejo Superior de Investigaciones Científicas/Universidad de Salamanca, Salamanca, Spain; [2]Laboratory of Electron Microscopy/Bio-imaging Center, Japan Women's University, Bunkyo-ku, Tokyo, Japan; [3]Integrated Imaging Research Support, Chiyoda-ku, Tokyo, Japan.

*M. Ramos and J.C.G. Cortés contributed equally to this paper;   Correspondence to Juan Carlos Ribas: ribas@usal.es;   Juan Carlos G. Cortés: cortes@usal.es.

ingression is generated by PS growth rather than by CR constriction, and that the rate of PS synthesis determines the rate of CR constriction and septum ingression (Proctor et al., 2012). However, in the same study, it was shown that LatA blocks the ingression of all the septa shorter than 50% of the total septum length. Moreover, some CR proteins persist longer than F-actin in cells treated with LatA and may play a role in septum ingression without F-actin (Naqvi et al., 1999; Wu et al., 2003; Thiyagarajan et al., 2015; Zhou et al., 2015). In addition, the absence of the Bgs4-synthetized major β(1,3)glucan causes a faster CR constriction than that of normal septa and a slower synthesis of the PS that lags behind the CR and ingressing membrane, and cannot provide the proposed pushing force for septum ingression (Muñoz et al., 2013; García Cortés et al., 2016). Thus, the roles of the CR, PS, and septum membrane throughout septation need to be reexamined in more detail.

Here, we have further investigated the role of these structures by simultaneously analyzing the CR, glucan synthases localization, and septum edge ultrastructure during septum ingression in cells deprived of F-actin by short and long LatA treatments (from 5 min to 3 h). Our study reveals the existence of two separate phases of septum ingression, which correlate with different structural and phenotypical properties of the septum: an initial slow-ingressing septum rudiment (≤0.30 μm), for which the F-actin is essential and LatA induces an immediate loss of the Bgs1 ring; and a fast-ingressing septum (>0.30 μm), in which the presence of F-actin is dispensable and where the Bgs1 ring persists much longer in the presence of LatA. Moreover, a detailed study of the septa longer than 0.30 μm revealed the dual function of the CR: it has (1) a landmark function dependent on the myosin-II heavy chain Myo2 and the formin Cdc12 to keep Bgs1 localized as a ring in the septum membrane edge and to maintain the septum shape, and (2) a contractile role. In addition, we describe and characterize many WT ingressing septa with the PS lagging behind the septum membrane edge. These findings show that fungal cytokinesis shares similarities with animal cytokinesis, requiring a centripetal CR and membrane closure, and with plant cytokinesis, requiring membrane addition as an important mechanism to drive cytokinesis.

Results

Fission yeast septation exhibits two consecutive phases with different ingression rates and levels of calcofluor staining

In fission yeast, septum ingression starts in early anaphase B, after CR assembly and maturation during metaphase and anaphase (Fig. 1, A and B; Cortés et al., 2018). The CR matures by sequentially acquiring new CR proteins until CR constriction and septation onset (Pollard and Wu, 2010; Kovar et al., 2011). CR constriction and septum ingression is not a uniform process, first occurring with a slow ingression rate and later increasing after telophase onset (Cortés et al., 2018).

Septum ingression and concomitant CR constriction start forming an incipient septum called the septum rudiment, in which only PS, made by the action of the glucan synthase Bgs1, is detected (Muñoz et al., 2013; Cortés et al., 2018). During ingression, the rudiment changes to a three-layered structure of

PS and SS due to the action of all the glucan synthases. The septum (comprising both the PS and SS) increases in thickness throughout ingression and by additional SS synthesis after completion (Fig. 1 C; Muñoz et al., 2013; Cortés et al., 2018).

We examined the septum length and time when the septum switches from slow to fast ingression by performing time-lapse video microscopy of WT cells stained with calcofluor white (CW), a fluorochrome that specifically stains the PS (arrow, Fig. 1 D; Cortés et al., 2007, 2018). Low-exposed CW images revealed a differential CW staining during septum ingression, with the septum rudiment exhibiting brighter fluorescence (arrow, Fig. 1 E; Fig. S1 A; and Video 1) and the ensuing septum exhibiting a weaker and more diffuse fluorescence (bracket, Fig. 1 E; Fig. S1 A; and Video 1). This weaker CW-stained septum was detected ~12–16 min after the first detection of the PS, and coincided with a switch in the septum ingression rate (3.5× increase), revealing two separate phases of ingression (Fig. 1, D, F, and G; Cortés et al., 2018). Quantification of the length of the CW-stained rudiment at the switch between ingression phases 1 (slow) and 2 (3.5× faster than phase 1) showed an average length of ~0.2–0.4 μm (Fig. 1, F and G). These results show that septation is not uniform and comprises two consecutive phases with different ingression rates that correlate with different CW staining patterns.

F-actin is essential for ingression of the phase 1 septum rudiments

It has been reported that F-actin is dispensable for ingression of septa that have reached >50% of total septum length (Proctor et al., 2012); however, the significance of F-actin during ingression of shorter septa is currently unknown. Thus, to understand the role of F-actin in the two phases of septation described above, we examined the septum ingression and morphology and glucan synthases localization in septa of different sizes and after short and long treatments with LatA (up to 3 h). For this purpose, GFP- and RFP-tagged glucan synthases and CW-stained septa were analyzed in cells grown in the presence of LatA for different periods of time. The fast disappearance of all F-actin structures in the presence of LatA (100 μM) was confirmed. After 5 min with LatA, no F-actin structure, including the actin ring, could be observed, and this absence continued after 30 min with LatA (Fig. S1 B).

Analyzing the septa according to the CW staining and glucan synthases localization for increasing periods of LatA treatment (Fig. 2 A and Fig. S1 C) showed a progressive decrease in the number of cells with a septum over time (Fig. 2 B and Fig. S1 D). The number of cells with open septa also decreased (open arrowhead, Fig. 2 A and Fig. S1, C and E), and only cells with complete septa (closed arrowhead) or with septum rudiments (arrow) remained over time with LatA (Fig. 2, A and B; and Fig. S1 C). The decrease in complete septa at longer times with LatA (Fig. S1 E) indicates that some of them were degraded because of cell separation (Fig. S2, A–D). These data corroborate the described finding that long open septa (>50% of its total length) are able to ingress to completion in the presence of LatA (Proctor et al., 2012), whereas septum rudiments do not progress. Thus, we were prompted to analyze the relevance of the septum length
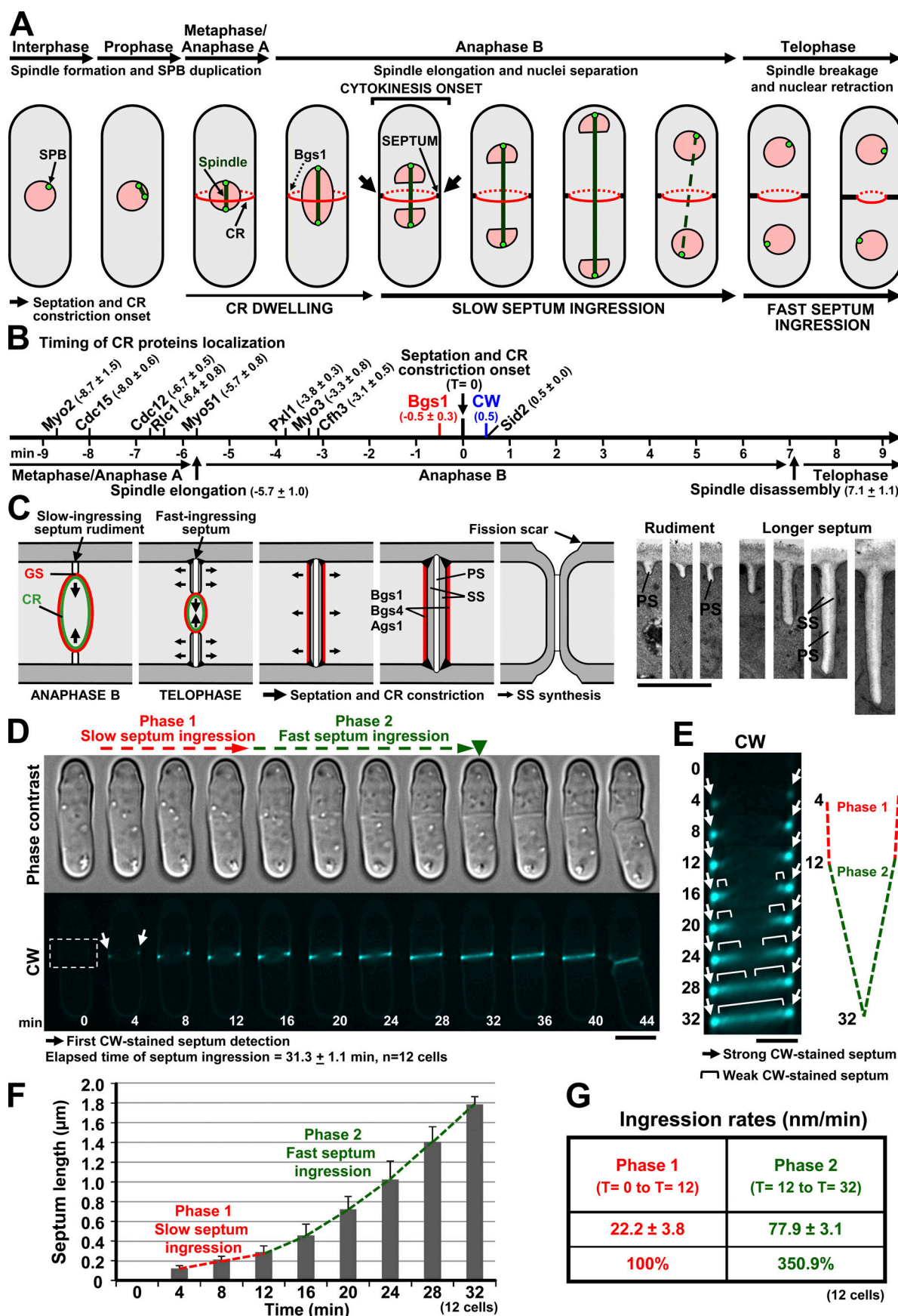
Ramos et al.
Two septation phases discriminated by Bgs1 with LatA

Journal of Cell Biology
https://doi.org/10.1083/jcb.201808163

4172

A Interphase | Prophase | Metaphase/Anaphase A | Anaphase B | Telophase

Spindle formation and SPB duplication · Spindle elongation and nuclei separation · Spindle breakage and nuclear retraction

CYTOKINESIS ONSET

SPB · Spindle · CR · Bgs1 · SEPTUM

→ Septation and CR constriction onset · CR DWELLING · SLOW SEPTUM INGRESSION · FAST SEPTUM INGRESSION

B Timing of CR proteins localization

Myo2 (-8.7 ± 1.5) · Cdc15 (-8.0 ± 0.6) · Cdc12 (-6.7 ± 0.5) · Rlc1 (-6.4 ± 0.8) · Myo51 (-5.7 ± 0.8) · Pxl1 (-3.8 ± 0.3) · Myo3 (-3.3 ± 0.8) · Cfh3 (-3.1 ± 0.5)

Septation and CR constriction onset (T= 0)

Bgs1 (-0.5 ± 0.3) · CW (0.5) · Sid2 (0.5 ± 0.0)

min -9 -8 -7 -6 -5 -4 -3 -2 -1 0 1 2 3 4 5 6 7 8 9

Metaphase/Anaphase A · Spindle elongation (-5.7 ± 1.0) · Anaphase B · Spindle disassembly (7.1 ± 1.1) · Telophase

C Slow-ingressing septum rudiment · Fast-ingressing septum · Fission scar · Rudiment · Longer septum

GS · CR · PS · SS · Bgs1 · Bgs4 · Ags1 · PS · SS · PS

ANAPHASE B · TELOPHASE · → Septation and CR constriction · → SS synthesis

D Phase 1 Slow septum ingression → Phase 2 Fast septum ingression

Phase contrast · CW

min 0 4 8 12 16 20 24 28 32 36 40 44

→ First CW-stained septum detection
Elapsed time of septum ingression = 31.3 ± 1.1 min, n=12 cells

E CW

0 4 8 12 16 20 24 28 32

4 Phase 1 12 Phase 2 32

→ Strong CW-stained septum
⌐ Weak CW-stained septum

F

Septum length (µm) vs Time (min)

Phase 1 Slow septum ingression · Phase 2 Fast septum ingression

(12 cells)

G Ingression rates (nm/min)

Phase 1 (T= 0 to T= 12)	Phase 2 (T= 12 to T= 32)
22.2 ± 3.8	77.9 ± 3.1
100%	350.9%

(12 cells)

Figure 1. **Septation comprises an evolving septum structure consisting of two consecutive phases with different ingression rates and levels of calcofluor staining. (A)** Model of the septum synthesis and formation of a cleavage furrow. Septation and CR constriction start in early–mid anaphase B with the activation of PS synthesis by the action of Bgs1 glucan synthase. Septum ingression is slow during anaphase B and increases during telophase (adapted from Cortés et al., 2018). **(B)** Scheme of the timing of the stable localization of different proteins as a ring at the cell middle with respect to the onset of septation and CR constriction (T = 0), first PS detection by CW staining (T = +0.5 min), and the mitotic phases (adapted from Cortés et al., 2018). **(C)** Model of septation (adapted from Muñoz et al., 2013). A PS incipient rudiment formed by the sole action of Bgs1 becomes a fast-ingressing septum during telophase, which is a three-layered structure formed by the simultaneous synthesis of PS and SS by the action of Bgs1, Bgs4, and Ags1. The septum increases in thickness throughout ingression, and the complete septum maturation proceeds by additional SS synthesis. Finally, cell separation proceeds by PS degradation, forming a fission scar. Right: TEM magnifications from rudiments to longer septa increasing in thickness throughout ingression are shown. Large arrow, direction of septum ingression and CR constriction; small arrow, direction of septum thickness increase; line points inside the CR, glucan synthase rings, PS, and SS. Scale bar = 1 µm. **(D)** WT septation showing two phases with different ingression rates and levels of CW staining. Early log-phase cells grown in YES at 28°C were examined by phase-contrast and CW staining time-lapse video microscopy. Arrows, first CW-stained septum detection; green arrowhead, septum completion (31.3 ± 1.1 min, n = 12 cells). Scale bar = 5 µm. **(E)** Kymograph of the CW-stained cell depicted in D (dashed rectangle). Arrows, phase 1 septum rudiment exhibiting brighter CW fluorescence; bracket, ensuing phase 2 longer septum with weaker CW fluorescence. A scheme of the septum progression during both ingression phases (phase 1, 4–12 min, and phase 2, 12–32 min) in the kymograph is shown. Scale bar = 2 µm. **(F)** Distinct progression of the septum length along the two ingression phases. The CW-stained septum length was quantified from time-lapse videos as in D, and the average septum length was calculated (n = 12 cells). **(G)** The septum ingression rates (nanometer/minute ± SD) were calculated for the indicated time intervals of phase 1 and 2 from time-lapse sequences as in D (n = 12 cells). GS, glucan synthase; SPB, spindle pole body. Error bars show SD.

for its ingression and completion in the absence of F-actin. Quantification of the septum length with increasing durations of LatA treatment showed that all open septa longer than 0.30 µm gradually disappeared, and after 1 h with LatA there were two major groups of septa: septum rudiments (0–0.30 µm) unable to ingress in the absence of F-actin, and complete septa (Fig. 2 B).

The special F-actin dependence of the septum rudiment ingression was analyzed both in cell population and in time-lapse video experiments. During all LatA treatments, the cells with septum rudiments always displayed the glucan synthases as large lateral bands in the plasma membrane of the cell middle, which increased over time instead of remaining concentrated, forming a ring at the septum edge (arrow, Fig. 2 C and Fig. S3 A). Time-lapse sequence analysis of RFP-Bgs1 rings in cells treated with LatA corroborated the finding that rudiments cannot ingress and cannot maintain Bgs1 concentrated at the septum edge in the absence of F-actin (arrow, Fig. 2 D). Bgs1 was, however, active and able to form CW-stained lateral cell wall depositions upon spreading from the initial CW-stained rudiment (arrowhead, Fig. 2 D).

The ultrastructure of the septum rudiments in cells treated with LatA was analyzed using transmission EM (TEM). The control cells (–LatA) showed a typical PS in rudiments and three-layered structures in longer open and complete septa that are composed of a PS flanked on both sides by the SS (Fig. 2 E), as previously described (Cortés et al., 2007, 2012; Muñoz et al., 2013; García Cortés et al., 2016). The LatA-treated cells with non-ingressing rudiments consistently showed large lateral cell wall depositions around the septum rudiments, indicative of active glucan synthases unable to perform septum ingression (arrow, Fig. 2 F). Thus, F-actin is essential for the slow ingression of septum rudiments (≤0.30 µm; Fig. 2 B), and its absence causes the spreading of glucan synthases, which form a remedial internal cell wall (ICW; Fig. 2 G) instead of the septum.

F-actin is dispensable for the ingression of phase 2 long septa

To understand why F-actin is dispensable for the ingression of longer septa (>0.30 µm, phase 2), we studied in more detail the ingression of these septa in the presence of LatA. It was observed that after short LatA treatments (5–15 min), most of the open septa maintained a normal thin shape under fluorescence microscopy, with the glucan synthases correctly localized to the septum edge (Fig. 3 A and Fig. S3 B). These results suggested the possible persistence of some CR proteins during LatA treatment that helped to maintain the glucan synthases localized as a ring. Time-lapse video microscopy of cells with septa longer than 0.30 µm (phase 2 of ingression) during short LatA treatments showed complete but slower ingression (middle and bottom panels, Fig. 3 B) than that of similar septa in cells without LatA (top panel, Fig. 3 B). Bgs1 remained localized as a ring at the septum edge during the entire ingression in the presence of LatA (Fig. 3 B), and this prompted us to examine the presence of CR myosin-II in these cells. Although F-actin structures disappeared quickly with LatA treatment (Fig. S1 B), myosin-II regulatory light chain Rlc1 remained during the entire septum progression until completion (green and blue arrowheads, Fig. 3 B). Consistent with previous reports, the Rlc1 ring was more stable than actin in the presence of LatA (Naqvi et al., 1999; Zhou et al., 2015). Rlc1, like other CR proteins, colocalized with the Bgs1 ring (Liu et al., 2002; Mulvihill et al., 2006; Pérez et al., 2016; Sethi et al., 2016; Figs. 1 C and 3 B, merge panels), and, therefore, the Bgs1 signal was used to define both CR constriction rate and septum membrane ingression rate.

Next, the ultrastructure of ingressing septa longer than 0.30 µm after short LatA treatments (5–15 min) was analyzed using TEM. Although these septa appeared to be normal under fluorescence microscopy (Fig. 3, A and B), they had altered ultrastructures with twisted PSs (Fig. 3 C), probably due to the misdirected ingression caused by the absence of CR tension. The septa ended with a sharp edge (arrow, Fig. 3 C), which is consistent with the observed Bgs1 ring at the septum edge of LatA-treated cells by fluorescence microscopy during similar times (Fig. 3, A and B). TEM also revealed slightly thicker open and complete septa, indicative of glucan synthases activity during the slower septum ingression (Fig. 3 C). In summary, short LatA treatments of ingressing septa (>0.30 µm, phase 2) promoted a slight reduction in the ingression rate, but the glucan synthase rings and at least CR Rlc1 remained until completion (Fig. 3 D).
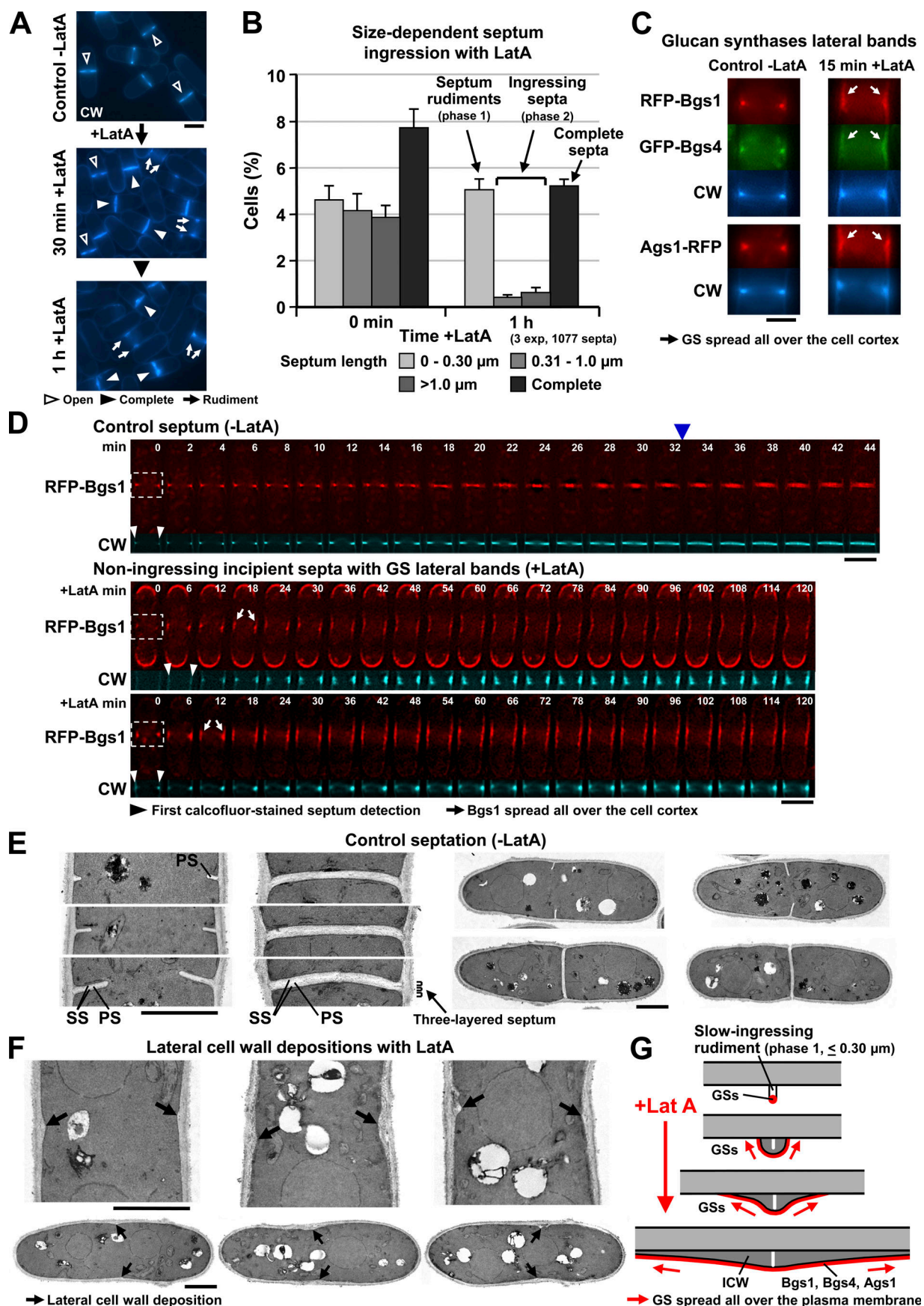
A

Control -LatA

CW

+LatA ↓

30 min +LatA

1 h +LatA

▷ Open ▶ Complete ➤ Rudiment

B

Size-dependent septum ingression with LatA

Septum rudiments (phase 1)
Ingressing septa (phase 2)
Complete septa

Cells (%)

Time +LatA

0 min | 1 h (3 exp, 1077 septa)

Septum length
0 - 0.30 μm | 0.31 - 1.0 μm
>1.0 μm | Complete

C

Glucan synthases lateral bands

Control -LatA | 15 min +LatA

RFP-Bgs1

GFP-Bgs4

CW

Ags1-RFP

CW

➤ GS spread all over the cell cortex

D

Control septum (-LatA)

min 0 2 4 6 8 10 12 14 16 18 20 22 24 26 28 30 32 34 36 38 40 42 44

RFP-Bgs1

CW

Non-ingressing incipient septa with GS lateral bands (+LatA)

+LatA min 0 6 12 18 24 30 36 42 48 54 60 66 72 78 84 90 96 102 108 114 120

RFP-Bgs1

CW

+LatA min 0 6 12 18 24 30 36 42 48 54 60 66 72 78 84 90 96 102 108 114 120

RFP-Bgs1

CW

▶ First calcofluor-stained septum detection ➤ Bgs1 spread all over the cell cortex

E

Control septation (-LatA)

PS

SS PS | SS PS | Three-layered septum

F

Lateral cell wall depositions with LatA

➤ Lateral cell wall deposition

G

Slow-ingressing rudiment (phase 1, ≤ 0.30 μm)

GSs

+Lat A

GSs

GSs

ICW Bgs1, Bgs4, Ags1

➡ GS spread all over the plasma membrane

Ramos et al.
Two septation phases discriminated by Bgs1 with LatA

Journal of Cell Biology   4175
https://doi.org/10.1083/jcb.201808163

Figure 2. **F-actin is essential for the ingression of incipient septum rudiments. (A)** Septation in cells treated with LatA. All the open septa (open arrowheads) except septum rudiments (arrows) progress to completion (closed arrowheads) in cells grown in the presence of LatA. Cells grown as in Fig. 1 D were shifted to YES containing LatA (100 µM; time 0) and analyzed by CW fluorescence microscopy. Scale bar = 5 µm. **(B)** The percentage of cells with septa divided into different length intervals as indicated was quantified in CW-stained cells as in A. After a long LatA treatment (1 h), most cells displayed either septum rudiments or complete septa (n = 1,077 septa). **(C)** LatA treatment in cells with septum rudiments causes Bgs1, Bgs4, and Ags1 glucan synthase spreading, forming large lateral bands (arrows). Cells were grown as in A and simultaneously analyzed by RFP, GFP, and CW fluorescence microscopy after 15 min with LatA. Scale bar = 2 µm. **(D)** Time-lapse sequences from incipient septation to completion in the absence of LatA (top panel) or from incipient septation to ingression arrest and spreading of Bgs1 in the presence of LatA (middle and bottom panels). Cells grown as in Fig. 1 D were shifted to YES containing LatA (time 0) and examined by RFP-Bgs1 and CW fluorescence time-lapse video microscopy. Arrows, loss of Bgs1 ring and spreading of Bgs1; white arrowheads, septum rudiment; blue arrowhead, septum completion; dashed rectangles, septum area shown in the time-lapse sequences of CW series. Scale bars = 5 µm. **(E)** TEM ultrastructure of control septa formed in cells without LatA treatment. Both open and complete septa present the typical three-layered structure of PS and SS. Cells were grown as in A without LatA and analyzed by TEM. Line points inside the PS and SS. Scale bars = 2 µm. **(F)** Ultrastructure of the lateral cell wall depositions (arrows) generated from non-ingressing septum rudiments without F-actin. Cells were grown as in A with LatA and analyzed by TEM. Scale bars = 2 µm. **(G)** Model of septum rudiment arrest and the ensuing lateral deposition of cell wall in the absence of F-actin. LatA treatment causes the blockage of slow-ingressing rudiments (phase 1, <0.30 µm in length) and Bgs1, Bgs4, and Ags1 spreading all over the plasma membrane, forming ICWs. GS, glucan synthase. Error bars show SD.

The absence of F-actin causes the spreading of the Bgs1 ring, which unveils a CR landmark function essential for the shape and ingression rate of phase 2 long septa

It was observed under fluorescence microscopy that after long LatA treatments (15–30 min), cells exhibited a new phenotype of thick aberrant septa (hereafter referred to as thick septa in contrast to thin septa) with the glucan synthases spread all over the septum membrane (arrow, Fig. 4 A). Quantification of this phenotype confirmed these observations of thick septa with Bgs1 spread (arrow, Fig. S3 C) and showed that open thick septa decreased over time, with complete thick septa appearing concomitantly. Thus, septum synthesis in the absence of both F-actin and the Bgs1 ring progressed to completion (Fig. S3 C). Time-lapse sequences of these cells demonstrated that thin ingressing septa switched to thick septa during LatA treatment (red arrowhead, Fig. 4 B). These thick septa completed ingression (blue arrowhead) at a much slower rate than that of both control septa without LatA and thin septa with LatA (Figs. 3 B and 4 B). The emergence of thick septa occurred immediately after the loss of the Bgs1 ring and its spread all over the septum membrane (arrow), despite the presence of the Rlc1 ring (Fig. 4 B and Fig. S3 D). These data suggest that Rlc1 is not the CR protein responsible for the landmark function that concentrates the glucan synthases as a ring in the absence of F-actin.

A more detailed analysis of the septum length and the timing of Bgs1 ring loss and thick septum formation indicated that septa longer than 60% of the total septum length (∼1.2 µm) at the time of LatA addition were able to complete cytokinesis as thin septa, whereas shorter septa, between 0.30 µm and 1.2 µm at the time of LatA addition, formed thick septa before completion (Fig. 4 C, left). During the time from LatA addition to Bgs1 ring loss and thick septum onset, which is ∼15 min (Fig. 4 C, middle), there was an average ingression of 0.47 µm, which corresponds to 24% of the total septum length (Fig. 4 C, right). Thus, all septa that require >15 min (or >0.47 µm) to reach completion will become thick in the presence of LatA.

The ultrastructure of the thick ingressing septa formed after different durations of LatA treatment (15–30 min and 2 h) was examined by TEM. After 15–30 min with LatA, most open septa appeared as thick blunt structures (arrow, Fig. 4 D and Fig. S3 E);

however, a few still presented the sharp edge of thin septa (arrowhead, Fig. S3 E). After 2 h in the presence of LatA, all the septa developed into much thicker structures (arrow) with twisted PSs (Fig. 4 E), probably due to a misdirected ingression caused by the loss of CR tension. In addition, an ICW layer was formed all over the septum, generating thicker five-layered septa (Fig. 4 E). Consistent with this observation, the new ends of the daughter cells formed after the separation of cells with five-layered septa maintained the ICW layer (Fig. S2 D). These data show that cells without both F-actin and glucan synthase rings are still able to maintain active glucan synthases along the septum membrane, and that at least some of the complete thick septa can eventually be degraded to become the pole of the new cell.

The rate of septum ingression and ring constriction in LatA-treated cells with thin and thick septa was analyzed in kymographs of RFP-Bgs1 time-lapse videos (Fig. 5 A), revealing two different, and likely consecutive, defective ingression rates (Fig. 5 B): first, a slow ingression rate of thin septa in the absence of F-actin (defective contractile function) but with persistent Bgs1 rings, which was half (51%) the septum ingression rate in control cells without LatA; and second, an extremely slow ingression rate of thick septa without both F-actin (defective contractile function) and Bgs1 rings (defective landmark function) that was 5% of the ingression rate in the control cells (Fig. 5, A and B). In summary, long LatA treatments promote a high reduction in the ingression rate of septa longer than 0.30 µm (phase 2) and the spreading of glucan synthases all over the septum membrane, which results in a very thick and atypical five-layered septum structure with PS, SS, and ICW (Fig. 5 C). Overall, our results show that CR F-actin is essential for the ingression of septum rudiments ≤0.30 µm (phase 1 of ingression; Fig. 5 D, 1), but dispensable for the ingression and completion of septa longer than 0.30 µm (phase 2 of ingression; Fig. 5 D, 2). Additionally, the ingression rate of septa longer than 0.30 µm without F-actin revealed two specific CR contributions to septum ingression: a role as a contractile structure, which exclusively depends on F-actin (Fig. 5 D, 2a and 2b), and a role as a spatial landmark, which is essential for both Bgs1 ring and septum morphology maintenance and depends not only on F-actin but on certain CR components (Fig. 5 D, 2a).
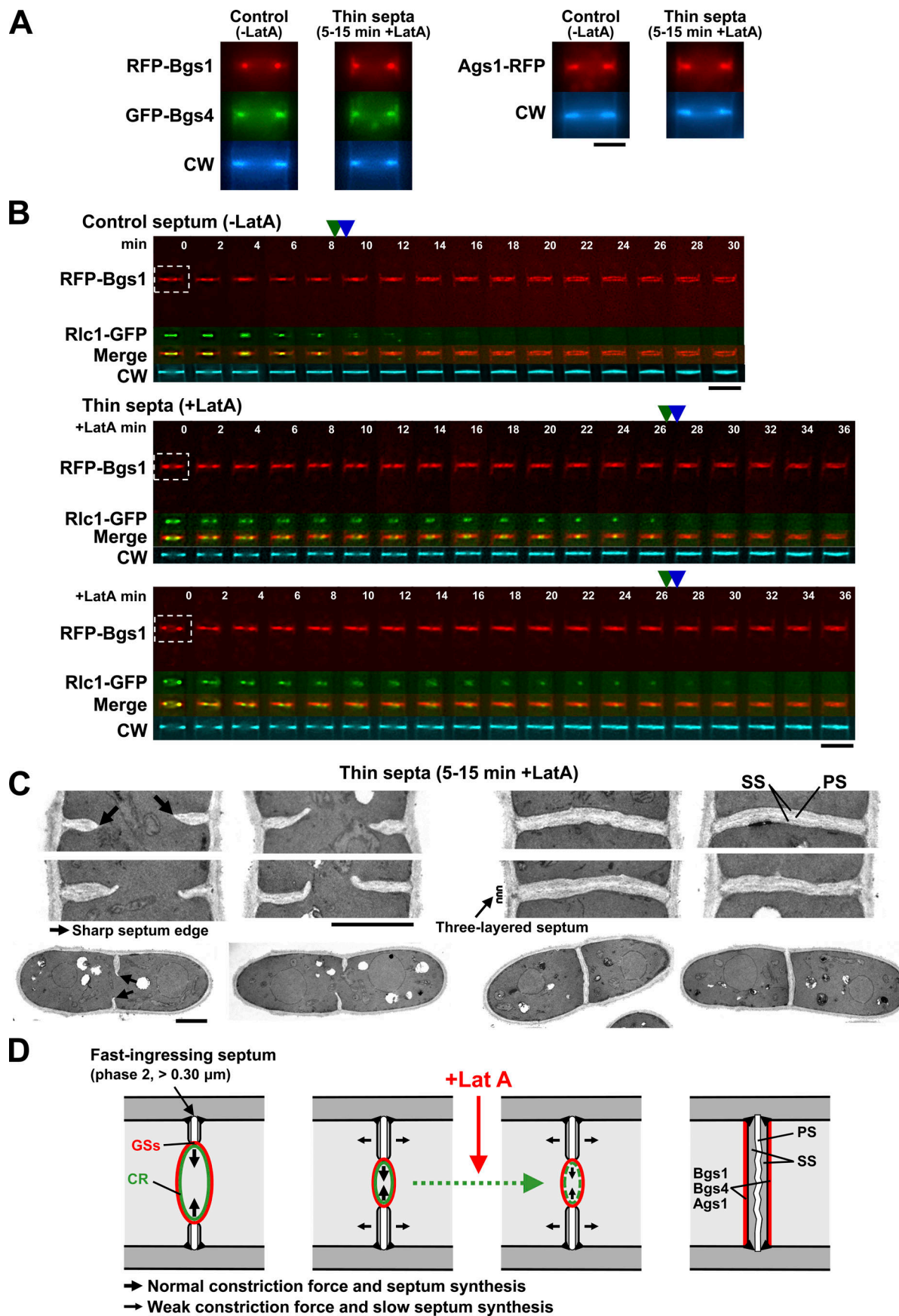
A

B

C Thin septa (5-15 min +LatA)

D

Figure 3. **F-actin is dispensable for the ingression of the longer septa of phase 2. (A)** After short LatA treatment (5–15 min), the longer septa of phase 2 remain thin and with Bgs1, Bgs4, and Ags1 correctly concentrated as a ring at the septum edge. Cells were grown in the presence of LatA and analyzed as in Fig. 2 C. Scale bar = 2 µm. **(B)** Time-lapse video microscopy of phase 2 septum ingression in cells grown either in the absence (control, top panel) or in the presence of LatA (middle and bottom panels). RFP-Bgs1, myosin-II regulatory light chain Rlc1-GFP, and CW fluorescence enabled the detection of the septum membrane, CR, and PS, respectively. Cells were grown in YES without or with LatA added at time = 0 and analyzed as in Fig. 2 D by RFP, GFP, and CW fluorescence microscopy. CR diameter at time = 0 measured as Rlc1 fluorescence was 0.61 µm (top panel), 0.64 µm (middle panel), and 0.81 µm (bottom panel). Dashed rectangles, septum area shown in the time-lapse sequences of Rlc1, Bgs1 and Rlc1 merge, and CW series; green arrowheads, Rlc1 ring loss; blue arrowhead, septum completion. Scale bars = 5 µm. **(C)** Ultrastructure of thin septa formed in cells after a short LatA treatment. The septa slightly increase in thickness and finish in a sharp edge (arrows). The PS is twisted, suggesting a misdirected ingression due to the absence of CR tension. Cells were grown as in Fig. 2 A in the presence of LatA and analyzed by TEM. The control septa formed without LatA are shown in Fig. 2 E. Line points inside the PS and SS. Scale bars = 2 µm. **(D)** Model of thin septum ingression in the absence of F-actin. Short LatA treatments in phase 2 ingressing septa (>0.30 µm in length) promote a slight reduction in the ingression rate, but the glucan synthase rings and CR Rlc1 remain until completion. GS, glucan synthase.

The CR landmark function responsible for the Bgs1 ring persistence in phase 2 septa specifically depends on the CR components Myo2 and Cdc12

Given that Rlc1 persisted after the loss of the Bgs1 ring in the presence of LatA, the localization of other CR proteins in cells treated with LatA was examined using time-lapse video microscopy (Fig. 6 A and Fig. S4 A). The loss of myosin-II heavy chain Myo2 (green arrowhead) was coincident with that of the Bgs1 ring (arrow) and with the appearance of thick septum morphology (red arrowhead, Fig. 6 A). In contrast, the other myosin-II heavy chain, Myo3/Myp2, and the myosin-V, Myo51, disappeared immediately after LatA addition (Fig. S4, A and B). In control cells without LatA, Myo2 and Myo51 localized to the CR until septum completion (blue arrowhead, Fig. 6 A and Fig. S4 A). The persistence of other CR proteins in the septum of cells treated with LatA was also analyzed in cell populations and compared with that of the Bgs1 ring (Fig. S4 B). A comparative examination enabled the classification of the CR proteins into three groups with different behaviors upon LatA treatment (Fig. 6 B): (1) low persistence, absent from the septum within 5 min with LatA (arrow), including F-actin, Myo3, and Myo51; (2) medium persistence, a marked decreased concentration at the septum after 15 min with LatA (arrow), including all glucan synthase rings, Myo2, and the formin Cdc12; and (3) high persistence, a decreased concentration only after 30 min with LatA (arrow), including paxillin Pxl1, the F-BAR homologue Cdc15, and Rlc1.

Likely CR proteins that are either absent before (Myo3 and Myo51) or remain in the septum after the emergence of thick septa (Pxl1, Cdc15, and Rlc1) in cells treated with LatA are not involved in the generation of these thick septa. In contrast, the loss of some CR proteins, such as Myo2 and Cdc12, which was coincident with the loss of the Bgs1 ring (Fig. 6 B), might trigger this Bgs1 loss, which in turn might cause the appearance of thick septa. In agreement with this hypothesis, the sole Bgs1 depletion (analyzed using a strain with bgs1+ expressed under the control of the lowest expression version 81X of the thiamine-repressible nmt1+ promoter, +thiamine, +T) was enough to produce thick septa similar to those observed in cells treated with LatA (arrow, Fig. 6 C and Fig. S4 C; Cortés et al., 2007). Moreover, these thick septa ingressed at a very slow rate similar to that of thick septa caused by LatA treatment (Fig. S4, D and E). However, in these thick septa generated by Bgs1 depletion, the CR proteins, including Myo2 and Cdc12, remained localized as a ring (arrow, Fig. 6 D and Fig. S5 A).

To examine the role of Myo2 and Cdc12 in the maintenance of the Bgs1 ring, myo2-E1 and cdc12-112 thermosensitive mutant cells were used to analyze by fluorescence microscopy the localization of Bgs1 and Cdc12 or Bgs1 and Myo2, respectively (Fig. 6 E). The loss of Myo2 function in myo2-E1 caused the progressive loss of Cdc12 and Bgs1 rings, as detected by measuring the fluorescence intensity of the residual Cdc12-YFP and RFP-Bgs1 rings (Fig. 6 E, right). Similarly, the absence of Cdc12 function in cdc12-112 produced a gradual loss of the Myo2-GFP and RFP-Bgs1 rings (Fig. 6 E, right). In both cases, the concomitant formation of a thick septum was observed (arrow, Fig. 6 E, left). Altogether, these data suggest that Myo2 and Cdc12 are responsible for Bgs1 ring localization, and that loss of the Bgs1 ring is responsible for the thick septum emergence and its slow ingression rate. In agreement with this, the thick septa generated in the absence of Myo2 or Cdc12 function were able to slowly ingress to completion, but septum degradation was impaired, resulting in a high accumulation of complete septa in the cells (Fig. S5 B).

All glucan synthase rings were lost with the appearance of thick septa in cells treated with LatA (Figs. 4 A and 6 B). However, while Bgs1 depletion caused the loss of Ags1 and Bgs4 rings and spreading of these proteins all over the membrane of thick septa (arrow, Fig. 6 F and Fig. S5 C), depletion of either Ags1 or Bgs4 (by using 81X-ags1+ or 81X-bgs4+ strains grown with thiamine, +T) promoted neither the loss of the Bgs1 ring nor the generation of thick septa (Fig. S5 D; Cortés et al., 2012, 2015; Muñoz et al., 2013). These data indicate that Bgs1 directs the localization of the other glucan synthases, Ags1 and Bgs4, but not the opposite, and suggest that Bgs1 delocalization is responsible for the spreading of Ags1 and Bgs4 throughout the septum membrane, which altogether cause the formation of thick septa.

In summary, these results confirm our finding of two separate roles for the CR: landmark and contractile functions (Fig. 6 G). Myo2 and Cdc12 contribute to the CR landmark function independently of its contractile function, in which both proteins likely participate. Both Myo2 and Cdc12 regulate the maintenance of Bgs1 as a ring, which in turn is the direct effector of the CR landmark function, concentrating the other glucan synthases (Fig. 6 G).

The Bgs1 ring exhibits a differential persistence in the septum edge during the two phases of septation in the presence of LatA

We have seen that fission yeast septation exhibits two consecutive phases with different ingression rates: phase 1 of
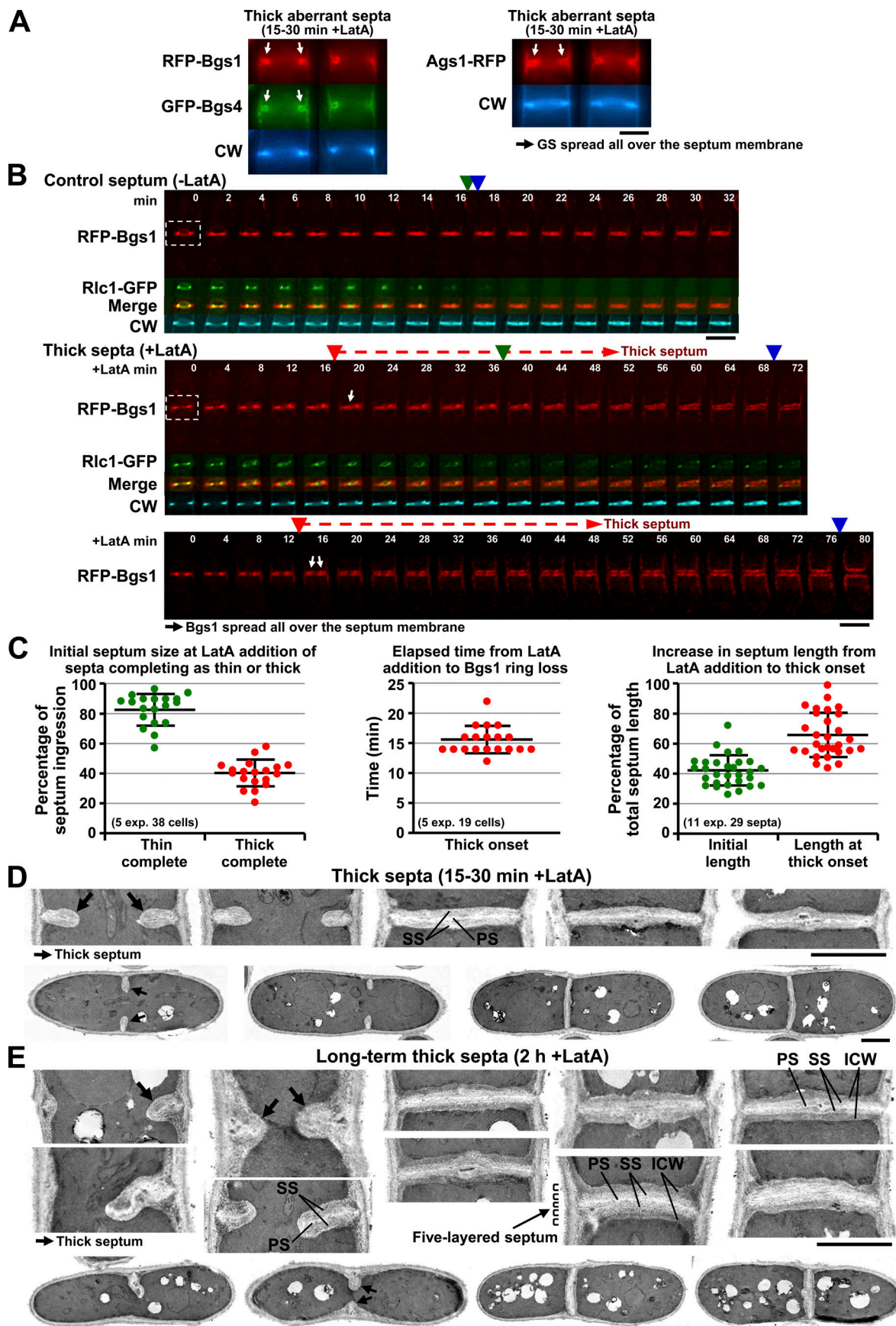
A Thick aberrant septa (15-30 min +LatA)

RFP-Bgs1

GFP-Bgs4

CW

Thick aberrant septa (15-30 min +LatA)

Ags1-RFP

CW

➔ GS spread all over the septum membrane

B Control septum (-LatA)

RFP-Bgs1

Rlc1-GFP
Merge
CW

Thick septa (+LatA) → Thick septum

RFP-Bgs1

Rlc1-GFP
Merge
CW

→ Thick septum

RFP-Bgs1

➔ Bgs1 spread all over the septum membrane

C

Initial septum size at LatA addition of septa completing as thin or thick

Elapsed time from LatA addition to Bgs1 ring loss

Increase in septum length from LatA addition to thick onset

D Thick septa (15-30 min +LatA)

SS PS

➔ Thick septum

E Long-term thick septa (2 h +LatA)

PS SS ICW

SS
PS

PS SS ICW

Five-layered septum

➔ Thick septum

Ramos et al.
Two septation phases discriminated by Bgs1 with LatA

Journal of Cell Biology   4179
https://doi.org/10.1083/jcb.201808163

Figure 4. The CR landmark function is essential for the maintenance of the glucan synthase rings, the shape, and the ingression rate of the phase 2 long septa. (A) After long treatments with LatA (15–30 min), the phase 2 ingressing septa became thick and aberrant, with Bgs1, Bgs4, and Ags1 spread all over the septum membrane. Cells were grown in the presence of LatA and analyzed as in Fig. 2 C. Scale bar = 2 μm. **(B)** The thick septa formed in cells treated with LatA can slowly ingress to completion. The emergence of thick septum morphology coincides with the loss of Bgs1 ring and the spreading of Bgs1 all over the septum membrane (arrows), but not with the loss of the Rlc1 ring, which remains for a longer period. Cells were grown and imaged using time-lapse video microscopy as in Fig. 3 B. Upper panel, control nontreated cells (CR diameter at time = 0 of Rlc1 = 0.81 μm); middle and lower panels, LatA-treated cells (middle, CR diameter at time = 0 of Rlc1 = 0.90 μm; bottom, Bgs1 ring diameter at time = 0 of 0.74 μm). Dashed rectangles, septum area shown in the time-lapse sequences of Rlc1, Bgs1 and Rlc1 merge, and CW series. Red arrowheads, thick septum onset; green arrowheads, Rlc1 ring loss; blue arrowheads, septum completion detected by RFP-Bgs1 septum membrane closure. Scale bars = 5 μm. **(C)** The length and timing of thin and thick septa were analyzed from time-lapse videos as in Fig. 3 B and Fig. 4 B. Images were captured at 2-min intervals. Left: septa longer than 60% of the total length at the time of LatA addition are completed as thin septa, whereas septa shorter than 60% of the length change morphology and are completed as thick septa (n = 38 cells). Middle: the Bgs1 ring loss and septum change to become thick occur ∼15 min after LatA addition (n = 19 cells). Right: the septum progression from the start of LatA addition to the Bgs1 ring loss and emergence of thick morphology is ∼24% of the total septum length (n = 29 septa). **(D and E)** Ultrastructure of thick septa formed after 15–30 min (D) or 2 h (E) of LatA treatment. The septa are thick, blunt structures (arrows) with twisted PSs, likely due to the absence of the Bgs1 ring (landmark defect) and to a contractile defect. The complete long-term thick septa (E) present an additional ICW probably made by Bgs1, Bgs4, and Ags1 spread all over the septum membrane, generating abnormal five-layered septa. Cells were grown in the presence of LatA as in Fig. 2 A and examined by TEM. The control septa formed without LatA are in Fig. 2 E. Arrows, whole thick septum structure; line points inside the PS, SS, and ICW. Scale bars = 2 μm. GS, glucan synthase. Bars in graphs show the average, and error bars indicate SD. Data distribution was assumed to be normal, but this was not formally tested.

slow-ingressing septum rudiments until they reach a length of ∼0.2–0.4 μm, and phase 2 of fast-ingressing septa (Fig. 1, F and G). In addition, we have described that after LatA treatment, the septum rudiments (≤0.30 μm) arrested ingression and the Bgs1 ring diffused to form Bgs1 lateral bands, whereas septa longer than 0.30 μm were able to ingress to completion and the Bgs1 ring persisted for a longer time (Figs. 2 and 3). To study the relationship between septum length and Bgs1 ring stability in the presence of LatA, we analyzed the presence of Bgs1 rings in septa of different sizes. We found that after 5 min in the presence of LatA, the Bgs1 ring was absent in all septum rudiments (≤0.30 μm; Fig. 7 A) but present in all ingressing septa longer than 0.30 μm (arrow, Fig. 7 A). Since the Bgs1 ring localization depended on Myo2 and Cdc12, we examined the persistence of these proteins in both rudiments and longer septa throughout LatA treatment and found it similar to that of Bgs1 (Fig. 7 B). These data show a differential persistence during LatA treatments of Bgs1, Myo2, and Cdc12 with respect to the septum size, which is coincident with the two different ingression rates and levels of CW staining detected under physiological conditions (Fig. 7 C).

Septum ingression in the absence of F-actin depends on Cdc42 GTPase and the exocyst complex

Besides Bgs1, other septum membrane proteins participate in septum synthesis and ingression, and, therefore, the chronological appearance in the middle of the cell of relevant septum proteins (green arrowhead), with respect to Bgs1 localization (red arrowhead) and septum synthesis (blue arrowhead), was determined by kymograph analysis of time-lapse videos (Fig. 8, A and B; and Fig. S6 A). The Bgs1 ring formed immediately before the onset of septation and CW detection during anaphase B as described previously (Cortés et al., 2018), whereas the rest of the analyzed proteins localized as diffuse patches or bands in the middle of the cell before the onset of septation (Fig. S6 A), and later, after the start of septation, they stably localized as a ring at the septum edge in a sequential fashion (Fig. 8 B). Next, we analyzed in cell populations whether the stable localization to the septum edge of each protein occurs during rudiment

maturation (≤0.30 μm) or after formation of mature septa (>0.30 μm). We observed that a given protein could be detected in similar sized septa either diffusely localized (open arrowhead) or as a stable ring (closed arrowheads, Fig. S6 B). Thus, the maximum septum length, with a diffuse localization of the protein, and the minimum septum length, with the protein localized as a ring, were determined for each of the selected proteins (Fig. S6 C). The coincidence of these two values was considered the septum length at which the protein is stably incorporated. As expected, the sequential protein localization according to the septum length correlated well with the order of protein localization determined by time-lapse video analysis (Fig. 8 B and Fig. S6 C). These analyses show that all septum proteins, except the anillin Mid2, localized during the maturation process of the rudiment (phase 1, Fig. S6 C), suggesting that any of those proteins could be responsible for the differential properties of phase 1 and 2 of ingression and for the switching to a stable septum in the presence of LatA.

Therefore, we examined the percentage of ingressing septa (>0.30 μm in length) in mutant cells defective for the different analyzed septum proteins and during different periods of LatA treatment (Fig. 8 C and Fig. S6 D). As a control, we confirmed that the ingression without LatA treatment of all the defective mutant strains (either nonessential deletions or thermosensitive mutants grown at the highest permissive temperature) proceeded as that of control cells under the assayed conditions. We found that Cdc42 GTPase, a major regulator of F-actin cable assembly and polarized secretion (Estravís et al., 2011), was essential for septum ingression in the presence of LatA (arrow, Fig. 8 C). Thus, arrest of septum ingression was observed in both cdc42-D76G and thermosensitive cdc42-L160S hypomorphic mutants (Estravís et al., 2011). The two Cdc42 guanine nucleotide exchange factors (GEFs) Gef1 and Scd1 promote cytokinesis via the differential activation of Cdc42 (Wei et al., 2016). We found that Gef1, but not Scd1, was critical for the ingression of septa lacking F-actin (arrow, Fig. 8 C and Fig. S6 D). The function of the BAR protein Hob3, which is required to localize Cdc42 to the septum (Coll et al., 2007), was also crucial for septum ingression with LatA. The Cdc42 effector kinase Shk1, but not Shk2, was
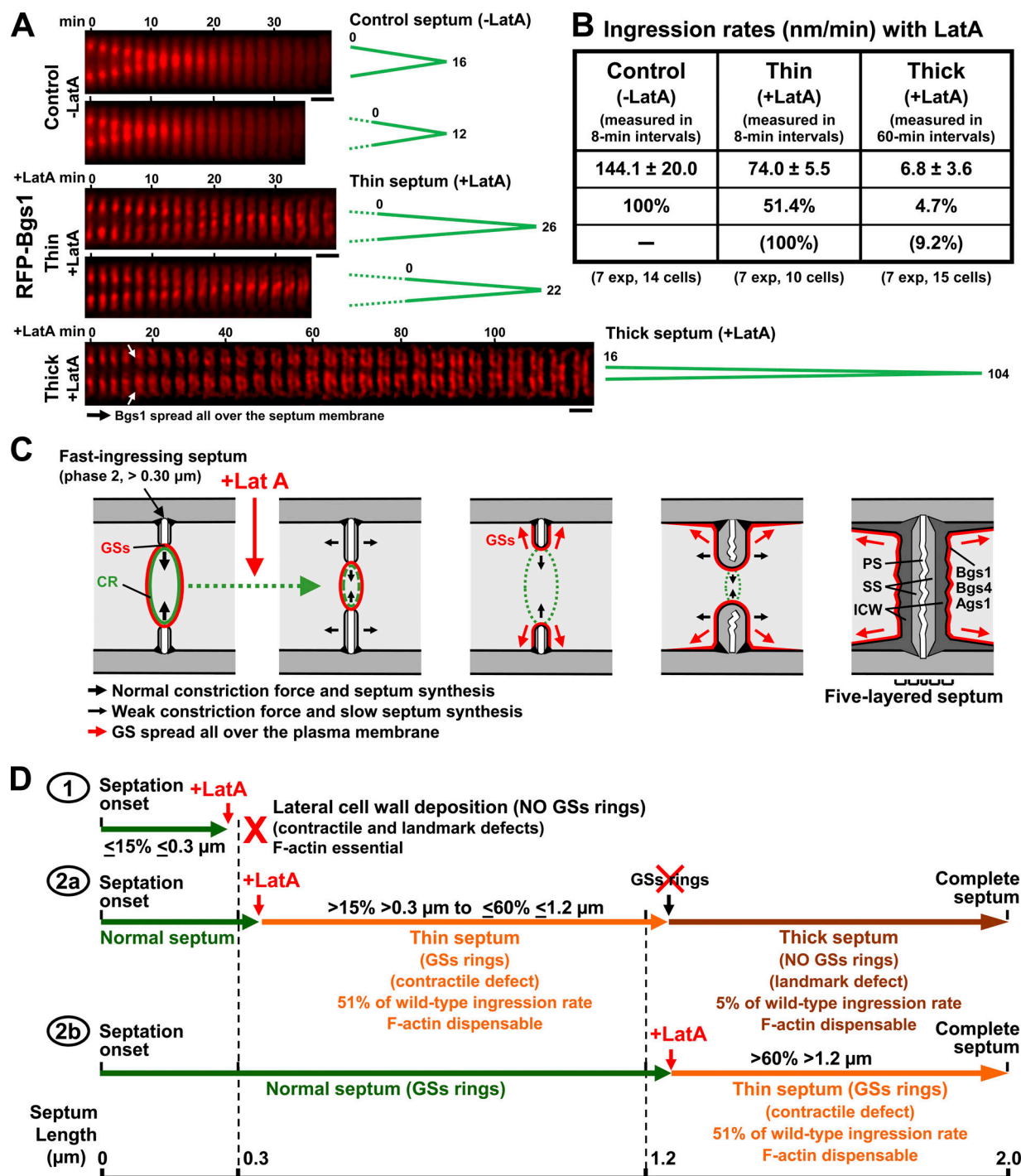
Ramos et al.
Two septation phases discriminated by Bgs1 with LatA

Journal of Cell Biology
https://doi.org/10.1083/jcb.201808163

4180

Figure 5. **Contractile and landmark dual contributions of the CR to septum ingression. (A and B)** Kymographs of Bgs1 time-lapse videos as in Figs. 3 B and 4 B (A) and ingression rates (nanometer/minute ± SD; B) of control (n = 14 cells) and LatA-treated cells with thin (contractile defect; n = 10 cells) and thick (landmark defect; n = 15 cells) septa. Arrows, Bgs1 ring loss and emergence of thick septum morphology. Scale bars = 2 µm. **(C)** Model of thick septum ingression in the absence of contractile (F-actin) and landmark functions of the CR. Long LatA treatment in phase 2 ingressing septa promotes loss of the glucan synthase rings and a concomitant severe reduction in the ingression rate. The glucan synthases spread all over the septum membrane, and the complete septum forms a very thick and atypical five-layered structure with PS, SS, and ICW. **(D)** Scheme of the essential (1), contractile (2a and 2b), and landmark (2a) contributions of the CR to septum ingression. In the presence of LatA (1), the defect caused by the lack of F-actin blocks the ingression of phase 1 rudiments, and the contractile (2a and 2b; F-actin loss) and landmark (2a; glucan synthase rings loss) dual defects promote a moderate and a severe reduction, respectively, in the ingression rate (51% and 5% of residual ingression rates) of phase 2 long septa. GS, glucan synthase.

A Control septum (-LatA)

B

C Control (-T)

GFP-Psy1

Bgs1 depletion (81X-bgs1+)
15 h +T   24 h +T

→ Thick septum

D Bgs1 depletion (81X-bgs1+ 24 h +T)
Myo2-GFP   Cdc12-YFP

→ CR proteins in thick septum

F Control (-T)   Bgs1 depletion (81X-bgs1+ 24 h +T)
GFP-Bgs4
CW
Ags1-GFP
CW

→ GS spread all over the membrane of thick septa

E myo2-E1   cdc12-112
25°C   28°C   25°C   36°C

→ Bgs1 spread all over the membrane of thick septa

Fluorescence intensity (A.U.)
myo2-E1 (28°C 10-24 h)   cdc12-112 (36°C 1-3 h)

G Contractile function   Landmark function

+LatA

CR → Actin ⤢ Myo2 / Cdc12 → Bgs1 ring → Bgs1 spread → Bgs4 ring → Bgs4 spread / Ags1 ring → Ags1 spread → Thick septum

Figure 6. **The CR landmark function is responsible for the Bgs1 ring persistence in the phase 2 septa and depends on the CR components Myo2 and Cdc12. (A)** The onset of thick septa in cells with LatA carrying RFP-Bgs1 and Myo2-GFP was analyzed by time-lapse video microscopy as in Fig. 3 B (bottom panel). In control cells without LatA treatment, Myo2 remains in the CR during the entire septum ingression (top panel). In cells with LatA, Myo2 is lost coincident with the loss of the Bgs1 ring (arrow) and the onset of thick septa (bottom panel). Dashed rectangles, septum area shown in the time-lapse sequences of Myo2-GFP and CW series; red arrowhead, thick septum onset; green arrowheads, Myo2 ring loss; blue arrowhead, septum completion. Scale bars = 5 µm. **(B)** The persistence of CR proteins and glucan synthase rings in cells treated with LatA was analyzed. Persistence was quantified as percentage of open septa with the corresponding protein localized as a ring at the septum edge at the indicated times of LatA treatment. The localization analysis enabled the classification of the studied proteins into three persistence categories: low (including F-actin; lost after 5 min), medium (including all glucan synthases; highly reduced after 15 min), and high persistence (reduced only after 30 min) in the presence of LatA. Differences in the persistence of each group are marked (arrows). All proteins were analyzed simultaneously using Bgs1 as a control. Cells were grown in the presence of LatA as in Fig. 2 C (n = 837 septa). **(C)** Bgs1 depletion generates thick septa (arrows). 81X-$bgs1^+$ cells carrying plasma membrane syntaxin GFP-Psy1 to visualize the septum thickness were grown in MM+S at 28°C and analyzed using GFP fluorescence microscopy at the indicated times of $bgs1^+$ repression with thiamine (+T). Scale bars = 5 µm. **(D)** Bgs1 depletion promotes thick septation with normal Myo2 and Cdc12 localization as a ring (arrows). Cells were grown and analyzed by fluorescence microscopy as in C. Scale bar = 2 µm. **(E)** Loss of Myo2 function causes the loss of Cdc12 ring and vice versa, and both equally generate the simultaneous Bgs1 ring loss and thick septation (arrows; left panels of septum details). The mutant cells $myo2-E1$ or $cdc12-112$ were grown in YES+S at 25°C, the temperature was shifted as specified, and the cells were analyzed by fluorescence microscopy. There is a gradual decrease in fluorescence intensity of the Bgs1 and Cdc12 rings in $myo2-E1$ thermosensitive mutant cells (n = 140 septa) and of the Bgs1 and Myo2 rings in $cdc12-112$ thermosensitive mutant cells (n = 149 septa; right panels). The Bgs1 ring vanishes and Bgs1 spreads all over the septum membrane after the Cdc12 or Myo2 ring disappears (dotted red line). Scale bars = 5 µm. **(F)** Bgs1 depletion promotes the loss of Bgs4 and Ags1 rings and the spread of these proteins all over the membrane of the thick septa (arrows, septum details). Cells were grown and analyzed as in C. Scale bars = 2 µm. **(G)** Scheme of the protein pathway involved in the contractile and landmark functions of the CR. Error bars show SD. Data distribution was assumed to be normal, but this was not formally tested.

also required (arrow, Fig. 8 C and Fig. S6 D). Similarly, the exocyst (Wang et al., 2016; Zhu et al., 2018) was essential for septum ingression in the presence of LatA, as observed by the arrest in septum ingression in the exocyst mutant $sec8-1$ (arrow, Fig. 8 C). The rest of the analyzed proteins were dispensable for septum ingression in the presence of LatA, since their absence did not alter the ingression rate, and sometimes even increased the rate (arrow, Fig. S6 D). The absence of Bgs4 causes an increase in the septum ingression rate (Muñoz et al., 2013), and the effects of the Bgs4 or Ags1 absence are very similar (Cortés et al., 2012). In accordance with this, the absence of Bgs4 or Ags1 promoted a decrease in the number of open septa with time in LatA (arrow, Fig. S6 D). Moreover, mutations in other proteins described to regulate Ags1 or Bgs4 (Rho2, Rho1, and the Rho-GEFs Rgf1 and Rgf3; Calonge et al., 2000; Tajadura et al., 2004; García et al., 2006) presented a similar decrease in open septa.

Overall, our data show that during phase 1 of slow ingression, the septum matures by the sequential incorporation of the septum membrane proteins, and during phase 2 of fast ingression, the septum is already mature. In this phase 2, Cdc42, its specific regulators (Gef1 and Hob3) and effector (Shk1), and the exocyst are essential for septum ingression in the absence of F-actin (Fig. 8 C).

Cytokinesis can progress with reduced or without PS at the septum edge

It has been proposed that cytokinesis is mainly driven by the pushing force of the growing PS synthesized by Bgs1 (Proctor et al., 2012). However, the observation that in cells depleted of Bgs4-dependent β(1,3)glucan, a defective PS can lag behind the septum membrane during ingression suggests that the addition of new membrane to the growing septum edge could be important for driving cytokinesis, at least in mutants with a defective PS (Muñoz et al., 2013; García Cortés et al., 2016). Since we have found the exocyst is essential for septum ingression without F-actin, and it has been suggested that an exocyst-

dependent expansion of the septum membrane is required for cytokinesis (Wang et al., 2016; Zhu et al., 2018), we used TEM to carefully examine the membrane deposition and septum edge ultrastructure in a high number of WT cells. A total of 122 TEM images of ingressing septa obtained from cells grown in different media from this study and 8 images from our previous studies (Cortés et al., 2012, 2015) were analyzed. We observed two different types of growing septum edges: 70 rounded and 60 sharp (Fig. 9 A). In the 70 rounded-edge septa, the PS covered the entire edge, and the PS edge limit (arrow) coincided with the septum membrane edge limit (arrowhead, Fig. 9 A, left). The 60 septa exhibiting a sharp edge had a much-reduced PS in the narrow sharp tip or even no detectable PS at the tip, indicating a delayed PS progression uncoupled from the membrane ingression. This in turn suggests that either SS or membrane addition, but not PS, can drive septum ingression (Fig. 9 A, right). Moreover, some recently completed septa (from 0.19 µm thickness) showed a thinner medial region without a PS, filled with a dark material or even with only the detectable membrane (Fig. 9 A, right; Cortés et al., 2012). However, all the mature complete septa analyzed (up to 0.42 µm thickness) presented a PS along the whole septum length, indicating that PS synthesis is not arrested in the sharp-edge septa, but instead lags behind membrane expansion during ingression.

A more detailed analysis of all the TEM images showed that the sharp septum edges can be classified into three types according to a gradual increase in the sharp edge phenotype (Fig. 9 B and Fig. S7, statistics included two images from Cortés et al., 2012): type 1, in which the thin PS edge (arrow) reaches the membrane edge (arrowhead) of the sharp septum, and the complete septa present a narrow medial region with PS; type 2, in which the PS edge does not reach the membrane edge, leaving a space filled by an electron-dense material resembling the SS, and the complete septa present a medial region without PS, filled with the electron-dense material; and type 3, in which the PS edge does not reach the membrane edge, leaving a space with no
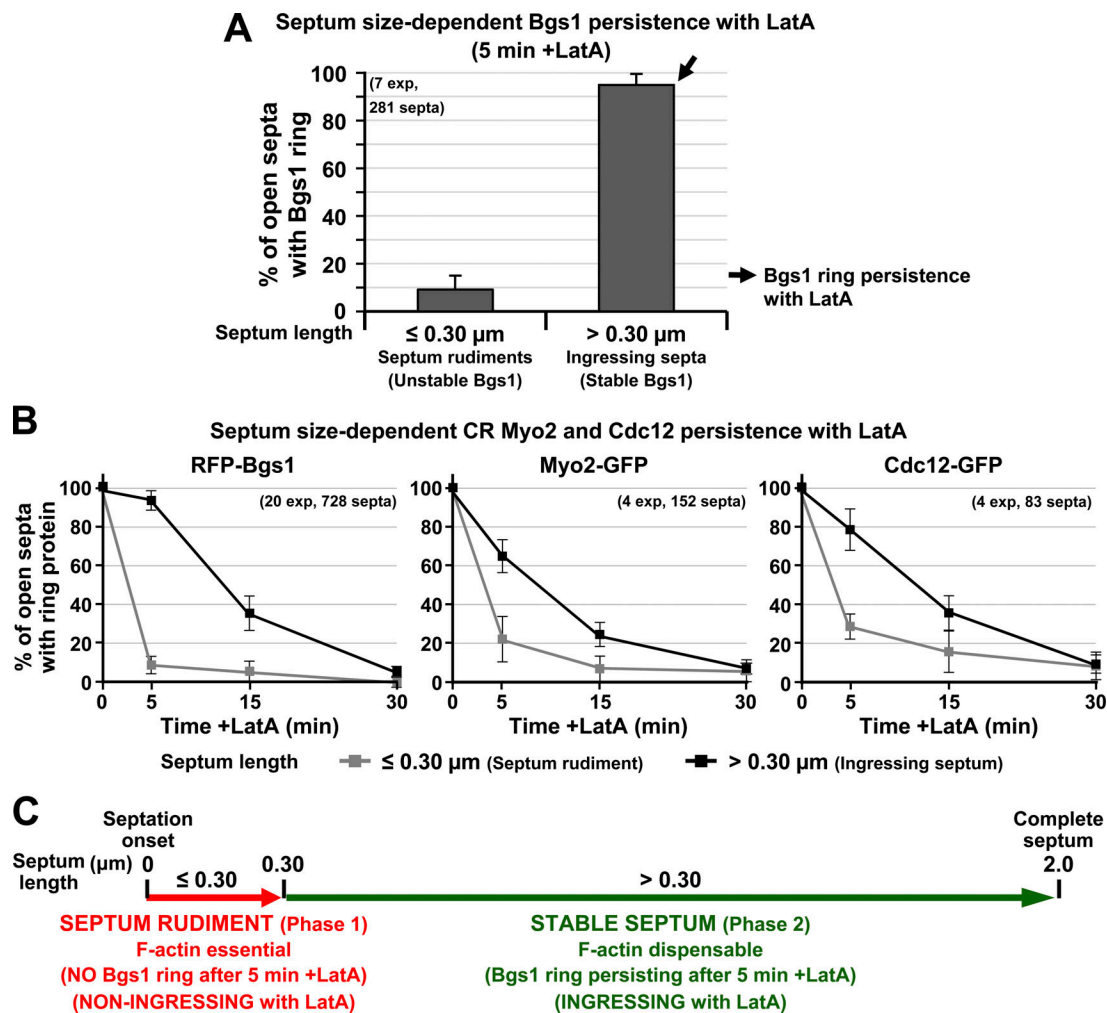
A Septum size-dependent Bgs1 persistence with LatA
(5 min +LatA)

B Septum size-dependent CR Myo2 and Cdc12 persistence with LatA

C

Figure 7. **The Bgs1 ring and CR proteins exhibit a differential persistence in the septum edge during the two consecutive septation phases in cells deprived of F-actin. (A)** Persistence of Bgs1 localization as a ring in cells after 5 min of LatA treatment (arrow). The percentage of open septa containing RFP-Bgs1 as a ring with respect to the septum length (measured by CW staining) was quantified. Bgs1 ring was found to be absent (Bgs1 spread) in phase 1 rudiments (≤0.30 µm) and still present (arrow) in phase 2 ingressing septa (>0.30 µm; n = 281 septa). **(B)** Myo2 and Cdc12 also display a dual persistence in cells treated with LatA. The persistence of Bgs1 (n = 728 septa), Myo2 (n = 152 septa), and Cdc12 (n = 83 septa) localizations as rings in either phase 1 rudiments or phase 2 ingressing septa was quantified as in A. **(C)** Scheme of the two successive septation phases in cells lacking F-actin: non-ingressing septum rudiment (≤0.30 µm, septum of phase 1) and ingressing longer septum (>0.30 µm, septum of phase 2). Error bars show SD.

septum material detectable by TEM, and the complete septa present a medial region without PS between both membrane layers (Fig. 9 B and Fig. S7).

The sharp septum edge structure was more frequent in cells grown in rich yeast extract with supplement medium (YES; 64% of total septa) and less frequent in cells grown in minimal medium with 1.3 M sorbitol (MM+S; 22% of total septa; Fig. 9 C, statistics included six images from Cortés et al., 2012, and two from Cortés et al., 2015). These differences might be due to the different growth rates (fastest in YES, slowest in MM+S), cell wall amounts (highest in YES, lowest in MM+S), or cell wall composition, which depends on the growth medium. Fluorescence microscopy analysis of many WT cells also enabled us to observe septa with complete membrane ingression, as detected by the localization of Bgs1 or the syntaxin homologue Psy1 (Maeda et al., 2009), but with open CW-stained PS (bracket, Fig. 9 D), similar to the complete septa without medial PS

observed by TEM, which likely originated from septa with a sharp edge (Fig. 9 A, right).

The existence of septa with uncoupled PS and septum membrane ingressions does not mean that PS synthesis is arrested; indeed, the PS will ultimately and necessarily be completed as observed by TEM, time-lapse video, and fluorescence microscopy (Fig. 9, A and D; Muñoz et al., 2013). We detected early complete septa (from 0.19 µm thickness) with or without PS in the septum middle region, which are much thinner than mature complete septa (up to 0.42 µm thickness), in which we never found incomplete PS. Therefore, PS synthesis is not arrested, but in some cases is delayed with respect to the membrane ingression, and during complete septum maturation, the PS is completed while the septum increases in thickness. This last stage of septum synthesis, even of PS material, must necessarily be performed by the glucan synthases along the septum membrane and by the glucan-modifying enzymes embedded in
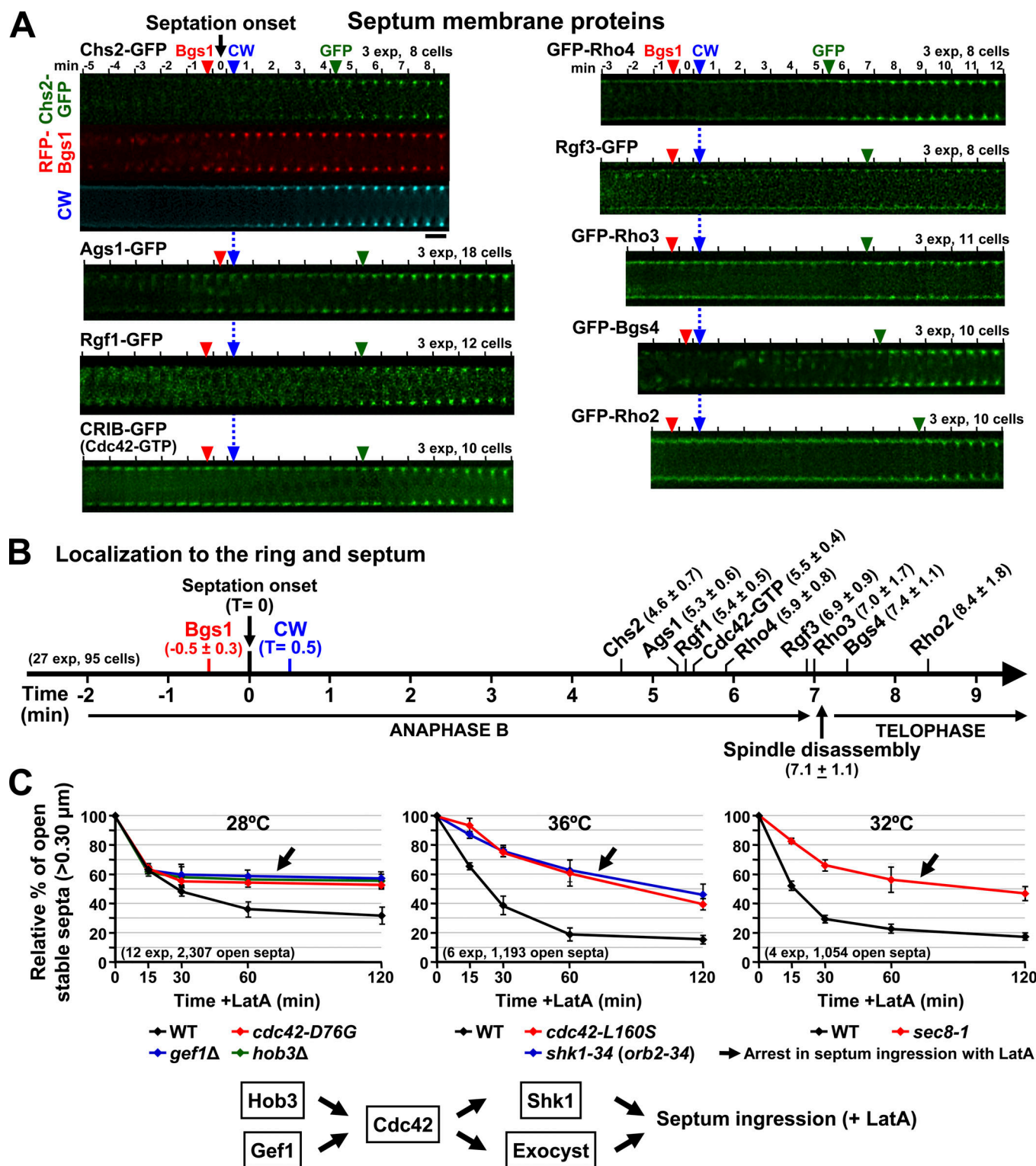
Figure 8. Septum ingression in the absence of F-actin depends on Cdc42 GTPase and the exocyst complex. (A) Kymographs of time-lapse videos to visualize the onset of stable localization of different septum proteins (green arrowheads) with respect to Bgs1 ring localization (red arrowheads) and the onset of septum synthesis (T = 0). Time = 0 was the time immediately before the first CW-stained septum detection (blue arrowheads). Cells were visualized by simultaneous GFP (septum protein), RFP (Bgs1), and CW (PS structure) fluorescence time-lapse video microscopy in each case (n = 95 cells). Kymographs simultaneously detecting chitin synthase homologue Chs2, Bgs1, and CW are shown as an example. For simplicity, only the GFP kymograph of the other analyzed proteins indicating the start of stable GFP localization (green arrowheads) is shown, and the corresponding RFP-Bgs1 and CW detections are shown by the red and blue arrowheads, respectively (RFP and CW kymographs not depicted). The kymographs were aligned with respect to the start of CW detection (blue arrowheads). Scale bar = 2 µm. **(B)** Scheme of the timing (minute ± SD) of stable localization of the analyzed septum proteins in the time-lapse video series from A with respect to the simultaneous localizations of the Bgs1 ring (red), onset of septation (T = 0), and detection of the CW-stained septum (T = +0.5,

blue; n = 95 cells). The timing of anaphase B, spindle disassembly, and telophase was selected from data previously reported in similar time-lapse video analyses (Cortés et al., 2018). **(C)** Cdc42 GTPase, Gef1 exchange factor, Hob3 BAR protein, Shk1 effector kinase, and the exocyst complex are essential for the ingression of phase 2 septa (>0.30 μm) in cells deprived of F-actin (arrows). The number of phase 2 open septa was quantified at the indicated times after treatment with LatA (n = 4,554 open septa). Values are the relative percentage of phase 2 open septa with respect to the total number of cells and were normalized, giving a value of 100% to the initial percentage of phase 2 open septa without LatA treatment. Cells were grown in YES at 28°C in the case of constitutive mutants, or at 25°C and shifted to the indicated temperatures in the case of thermosensitive mutants, transferred to YES containing LatA and analyzed by RFP-Bgs1 and CW fluorescence microscopy. The temperatures used correspond to the highest permissive temperature at which the septum ingression of thermosensitive mutant cells and control WT cells without LatA treatment proceeded as normal (not depicted). A scheme of the protein pathway involved in the control of septum ingression is shown. CRIB, Cdc42/Rac-interacting binding (probe for active Cdc42-GTP). Error bars show SD.

the septum wall to extend, modify, and cross-link the polysaccharides to their final complex structures (Cabib and Arroyo, 2013; Free, 2013; Mouyna et al., 2013; Gow et al., 2017).

Overall, these data show that the septum can progress with coincident PS and membrane edges, forming a rounded septum edge (Fig. 9 E, left), or with reduced or even delayed PS synthesis with respect to the ingressing membrane, forming three types of sharp septum edges according to a gradual increase in the sharp edge phenotype (Fig. 9 E, right). In both cases, rounded and sharp edges, septum ingression proceeds with the aid of the contractile function of the CR (arrow, Fig. 9 E), which maintains membrane tension, and with the landmark function of the CR, which maintains the glucan synthase rings and directs the deposition of vesicles and membrane expansion (circle, Fig. 9 E). Since the PS edge can advance coupled to, or delayed with respect to, the ingressing membrane edge, PS synthesis might not necessarily be the driving force of septum ingression.

Discussion

In fission yeast, septum ingression is not uniform but starts with a slow rate during anaphase B that increases after the onset of telophase (Cortés et al., 2018). It has been proposed that glucan synthesis by Bgs1 in the growing PS edge could provide the major force required to drive septum ingression, whereas the contractility of the CR might be largely dispensable (Johnson et al., 2005; Proctor et al., 2012). However, the contractility of the CR is still important for the overall septum ingression process, since it was shown that only septa longer than 50% of total length can slowly ingress to completion when the septum is devoid of actomyosin-dependent contractility (Proctor et al., 2012). Therefore, we were prompted to study the septation mechanism in the absence of F-actin and reexamine the role of the CR in the localization of glucan synthases during both phases of septum ingression.

Septum ingression comprises two consecutive phases of septum rudiment and long stable septum, each of them with different structural and phenotypical properties

Our results showed that the two described septum ingression rates correlate with two consecutive phases of septation, which exhibit different levels of CW staining and septum maturation: phase 1, where the septum proteins are sequentially incorporated in a septum rudiment; and phase 2, where all the septum proteins have already been recruited in a mature septum. In addition, the septum shows structural differences between both phases when analyzed by TEM: the rudiment ultrastructure only

shows a PS, whereas the ingressing septum permits discrimination of both the PS and SS (Muñoz et al., 2013). We also found that these septation phases exhibit a distinct behavior in the presence of LatA: (1) septum rudiments, ≤15% of the septum length (≤0.30 μm), showed very unstable glucan synthase rings and were unable to ingress; and (2) longer septa, >15% of the septum length (>0.30 μm), with more stable glucan synthase rings and able to ingress (Fig. 7 C). Overall, these findings are consistent with previous studies (Cortés et al., 2018). Similarly, during Drosophila cellularization, the CR constriction is biphasic, with a significantly slower initial constriction rate (Royou et al., 2004). This could be due to the plasma membrane expansion events required for furrowing at this stage, as has been proposed for the embryo (Figard et al., 2013; Wei et al., 2016).

Our findings, however, are not in agreement with the previous conclusion that only those septa longer than 50% of the total length are able to ingress without F-actin (Proctor et al., 2012). This discrepancy could be due to the protocols used at that time. In the previous work, septum ingression in the presence of LatA was only examined by time-lapse video during short times (up to 40 min), whereas in this study it was studied from short to long times with LatA (from 5 min to 3 h) by both time-lapse video and cell population analyses. During the applied LatA treatments, only one cell cycle took place, with the cells arresting in interphase after septation. Therefore, the observed septa are reflecting a sole cell division process occurring during the LatA treatment. Only the septa able to complete ingression in a short time in the presence of LatA were described in the previous study, and those correspond to the thin septa described here longer than 60% of the total length. The thick septa with spread glucan synthases were not described in the previous study because they ingress at an extremely slow rate and cannot complete septation during short times with LatA (up to 40 min). Here, we show that all septa longer than 15% of the total length progress to completion in the presence of LatA, initially fast, but after 15–20 min of LatA treatment, they become slow ingressing and thick. Therefore, only those septa longer than 60% of the total length can complete a fast ingression before this change occurs.

Cdc42 plays a central role in the establishment of polarized growth and membrane trafficking; however, its role in cytokinesis is less well understood. We found that the exocyst and Cdc42 are essential for the ingression of septa in cells treated with LatA. It has been described that Gef1 promotes the onset of CR constriction and septum synthesis (Wei et al., 2016). Here we show a new function of Gef1, but not of the main Cdc42 GEF Scd1, that takes place after the septum rudiment maturation
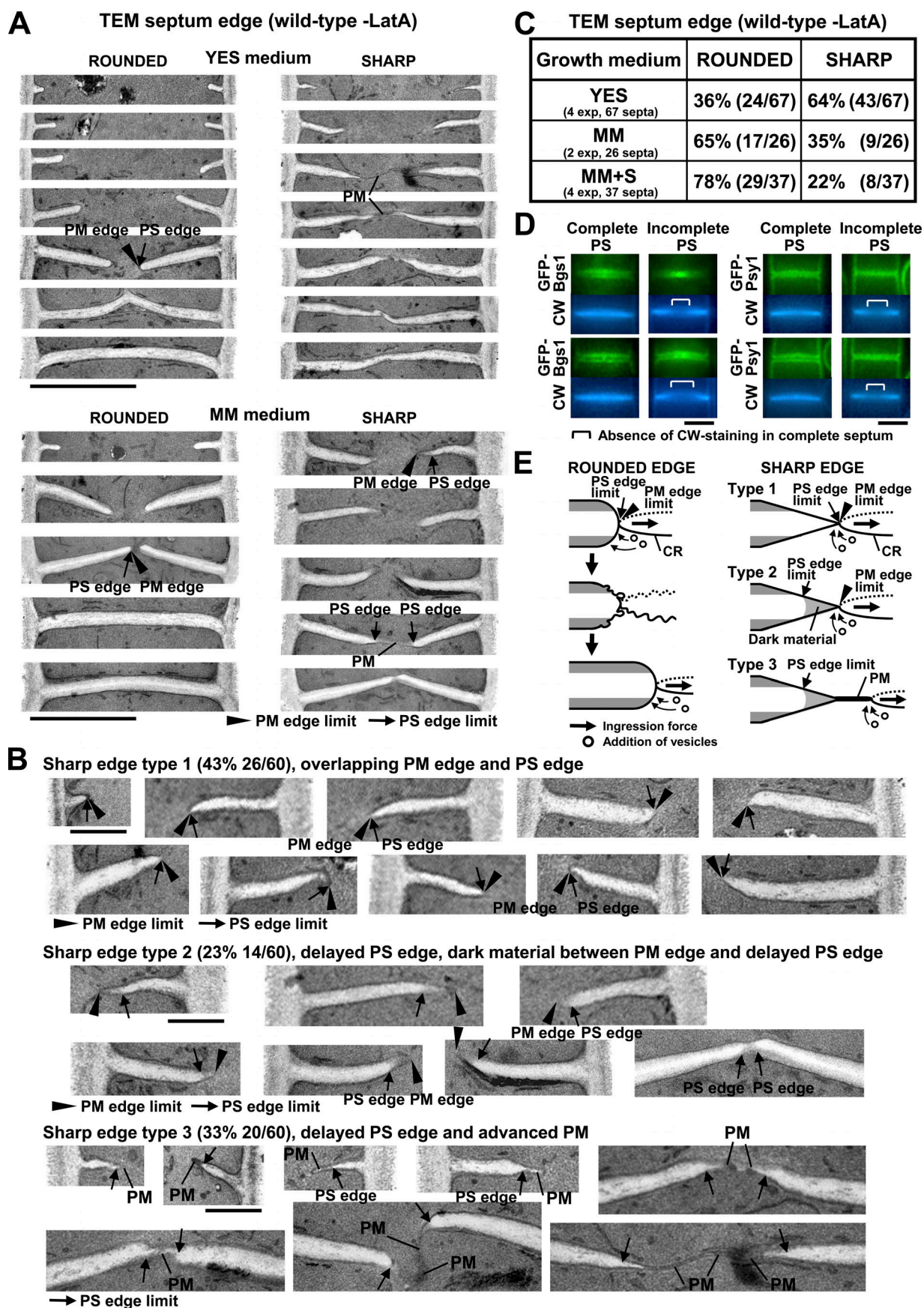
A TEM septum edge (wild-type -LatA)

YES medium — ROUNDED / SHARP

PM edge PS edge
PM

MM medium — ROUNDED / SHARP

PS edge PM edge
PM edge PS edge
PS edge PS edge
PM

► PM edge limit → PS edge limit

C TEM septum edge (wild-type -LatA)

Growth medium	ROUNDED	SHARP
YES (4 exp, 67 septa)	36% (24/67)	64% (43/67)
MM (2 exp, 26 septa)	65% (17/26)	35% (9/26)
MM+S (4 exp, 37 septa)	78% (29/37)	22% (8/37)

D

Complete PS / Incomplete PS — GFP-Bgs1 / CW
Complete PS / Incomplete PS — GFP-Psy1 / CW
GFP-Bgs1 / CW
GFP-Psy1 / CW

⌐ Absence of CW-staining in complete septum

E

ROUNDED EDGE
PS edge limit PM edge limit
CR

SHARP EDGE
Type 1 PS edge limit PM edge limit CR
Type 2 PS edge limit PM edge limit Dark material
Type 3 PS edge limit PM

→ Ingression force
○ Addition of vesicles

B

Sharp edge type 1 (43% 26/60), overlapping PM edge and PS edge

PM edge PS edge
► PM edge limit → PS edge limit
PM edge PS edge

Sharp edge type 2 (23% 14/60), delayed PS edge, dark material between PM edge and delayed PS edge

PM edge PS edge
► PM edge limit → PS edge limit
PS edge PM edge
PS edge PS edge

Sharp edge type 3 (33% 20/60), delayed PS edge and advanced PM

PM
PM
PM
PS edge PS edge PM
PM
PM PM
→ PS edge limit
PM PM

Figure 9. **Cytokinesis can progress with reduced or without PS at the septum edge. (A)** The analysis of the ultrastructure of ingressing septa from WT cells (n = 130 septa) reveals two types of growing septum edges: rounded (54%) and sharp (46%). Many sharp septa present a delayed PS edge (arrows) uncoupled from the plasma membrane edge (arrowheads) and CR ingression. The recent complete septa (from 0.19 µm thickness) sometimes present a narrow medial region without a PS, indicating a previous sharp septum edge lacking a PS. Cells were grown in either YES or MM at 28°C and examined by TEM. Scale bars = 2 µm. **(B)** Magnifications of sharp septum edges in TEM images as in A. The sharp septum edges can be classified into three types according to a gradual increase in the sharp edge phenotype: type 1, overlapping PS and plasma membrane edges, the PS reaches the edge of the sharp septum; type 2, delayed PS edge with respect to the plasma membrane edge, leaving a space filled by a dark material similar to that of the SS; and type 3, advanced plasma membrane with no detectable PS material between both plasma membrane layers. The percentage and number of each type of sharp edge with respect to the total number of analyzed sharp edges (n = 60 sharp septum edges) are shown in parentheses (statistics include two images from Cortés et al., 2012). Images are from cells grown in different media as in A. Scale bars = 1 µm. **(C)** Quantification of rounded and sharp septum edges with respect to the growth medium of cells analyzed by TEM as in A (statistics include six images from Cortés et al., 2012, and two from Cortés et al., 2015). The number of each type of septum with respect to the total number of analyzed septa is shown in parentheses (YES, n = 67 septa; MM, n = 26 septa; MM+S, n = 37 septa). **(D)** Septa detected as complete by plasma membrane Bgs1 or syntaxin Psy1 localization present either complete or open PS (brackets) as detected by CW staining, similar to the complete septa observed by TEM in A. WT cells grown as in Fig. 1 D were analyzed by fluorescence microscopy as in Fig. 2 C. Scale bars = 2 µm. **(E)** Model of the ingression of both rounded and sharp septum edges. The addition of membrane vesicles allows the increase in plasma membrane surface and the decrease in CR tension (arrows). CR constriction coupled to septum plasma membrane and PS depositions permits overlapping plasma membrane and PS edges to make a rounded septum edge. CR constriction coupled to plasma membrane ingression but with reduced or delayed PS deposition generates a sharp septum edge, which can be classified into three types according to a gradual increase in the sharp edge phenotype, as described in B. PM, plasma membrane. Arrow, limit of PS edge; arrowhead, limit of septum membrane edge. Line points inside the septum membrane structure.

process and is essential for the ensuing ingression of the stable septum in the absence of F-actin. In budding yeast, Cdc42 is active during anaphase, and its activity drops during mitotic exit and the onset of septation (Atkins et al., 2013; Onishi et al., 2013). In contrast, fission yeast GTP-bound Cdc42 remains as a diffuse band in the middle of the cell during most of anaphase B (slow-ingressing rudiment), but localizes to the septum membrane later in telophase during fast septum ingression. Active Cdc42 provides a landmark interacting with the exocyst for vesicle fusion to the plasma membrane (Pérez and Rincón, 2010; Estravís et al., 2011; Heider and Munson, 2012). It is possible that the CR also plays a prominent role in determining normal septum membrane ingression and the Cdc42–exocyst pathway would be more prevalent in the absence of F-actin.

The differential ingression rate of phase 2 long septa in cells lacking F-actin relies on Cdc12 and Myo2-dependent maintenance of the Bgs1 ring

Our time-lapse videos and cell population studies after short and long LatA treatments indicate that although the CR is not essential for ingression and completion of septa longer than 0.30 µm, its absence critically affects the septum ingression rate. First, the absence of F-actin in phase 2 long septa causes a contractile defect that maintains thin septa with glucan synthase rings in the edge but reduces the ingression rate, which is two times slower than the normal rate, in agreement with previous data (Proctor et al., 2012). Second, prolonged LatA treatment in phase 2 septa causes a landmark defect triggered by the loss of Myo2 or Cdc12 that in turn causes loss of the Bgs1 ring and the spreading of Bgs1 and, as a consequence of this, the spreading of Ags1 and Bgs4 all over the septum membrane. The diffusion of glucan synthases as a whole triggers the formation of thick septa. In agreement with these observations, we show that repression of bgs1⁺, but not of bgs4⁺ or ags1⁺, produces thick septa similar to those observed with LatA, even if the CR remains localized to the septum edge. In summary, during cytokinesis the CR plays two essential roles: as a spatial landmark and as a contractile structure. As a landmark, it participates in the

recruitment of Bgs1 into a ring, which is essential for the onset of septum synthesis, in the maturation and ingression of septum rudiments (phase 1), in the maintenance of the Bgs1 ring at the edge of ingressing mature septa (phase 2), and in the recruitment of the exocytic vesicles required for new membrane addition (Wang et al., 2002, 2016; Vjestica et al., 2008; Juanes and Piatti, 2016; Bhavsar-Jog and Bi, 2017; Zhu et al., 2018). In its role as a contractile structure, it is also necessary as a safety closing belt mechanism that maintains the membrane tension required for a straight septum ingression (Muñoz et al., 2013; García Cortés et al., 2016).

Cytokinesis can progress with undetectable pushing by the PS at the growing septum edge

It has been suggested that synthesis of PS provides the major force required to drive septum ingression (Proctor et al., 2012; Zhou et al., 2015) and also the opposite, that PS synthesis is insufficient to generate constriction and septum ingression (Cheffings et al., 2016). In addition, it has been described that the absence of Bgs4-synthesized β(1,3)glucan causes both delayed PS progression and faster CR and membrane ingression than that of WT septa (Muñoz et al., 2013; García Cortés et al., 2016). Here, we show by both TEM and fluorescence microscopy that uncoupled PS synthesis and septum membrane ingression also occur in WT cells, although less frequently than in cells depleted of Bgs4. Our TEM analysis of 130 WT septa showed many septa where the PS edge is behind the septum membrane edge. These sharp-edge septa point to septum membrane ingression occurring with a reduced or nonexistent pushing force from the PS, likely by addition of exocytic vesicles and membrane edge expansion (Vjestica et al., 2008; Wang et al., 2016; Zhu et al., 2018), as has been shown in animal and plant cytokinesis (Albertson et al., 2005; Prekeris and Gould, 2008; Müller and Jürgens, 2016; Smertenko et al., 2017). The PS synthesis is not necessarily performed from the Bgs1 ring at the septum edge. Bgs1 and the rest of the glucan synthases also localize throughout the septum membrane, and, therefore, septum synthesis is also performed along the septum, growing inward and increasing

simultaneously the thickness of both the PS and SS (Fig. 1 C; Cortés et al., 2002, 2005, 2012; Muñoz et al., 2013). It is hard to imagine how a tiny PS synthesis in the narrow sharp tip (type 1, 20% of analyzed septa) would provide the ingression force for the whole septum width. In addition, if pushing by the PS were necessary for ingression, the membrane edge would never separate and advance further than the PS edge (as observed in types 2 and 3 of sharp septum edges, which together account for 26% of the analyzed septa). Type 3 of sharp septum edges seems to be more abundant during the late stages of septum ingression; this suggests that coupled septum (PS and SS) and membrane ingressions could be more critical in the early stages of septation.

In addition, the fact that many septa imaged through different techniques of EM were observed to exhibit sharp edges in previously published studies (at least 18 previous studies and 39 images) confirms that the three types of sharp septum edge described here are not mere artifacts caused by fixation and dehydration for TEM imaging (Johnson et al., 1973; Kanbe et al., 1989, 1993; Mateos and Domínguez, 1991; Arai et al., 1998; Barnett and Robinow, 2002; Nakano et al., 2003; Donoso et al., 2005; Osumi et al., 2006; Cortés et al., 2012; Jourdain et al., 2012; Osumi, 2012; Pollard et al., 2012; Muñoz et al., 2013; Oberti et al., 2015; Davidson et al., 2016; Sipiczki, 2016; Wang et al., 2016).

Our results suggest that the contributions of total septum growth (PS and SS) and membrane addition to furrow ingression are more important than PS contribution. On the other hand, the thick slow-ingressing septa formed in the absence of Bgs1 and with the CR localized suggest that Bgs1 and the PS it synthesizes play an important role in determining the rate of septum ingression. Although in the absence of Bgs1 the CR is localized, it is unknown whether it is functional or not. Supporting a possible CR regulation by Bgs1, it has been described that the cps1-191 mutation of Bgs1 causes unstable CR, and also that Bgs1 cooperates with CR proteins in the septum formation (Cortés et al., 2015; Martín-García et al., 2018). A possible explanation is that Bgs1 and/or the PS, together with the CR, are a landmark for membrane addition during septation. If Bgs1 absence, a nonfunctional CR, or both cause a landmark defect impeding the vesicle fusion required for septum ingression, this would explain the low rates of septum ingression of the thick septa even in the presence of high levels of glucan synthases. This function would also be compatible with the existence of many WT septa with detached PS, lagging behind the septum membrane edge, and would explain the arrest in septum ingression with LatA of defective Cdc42 and exocyst mutants.

Overall, our results suggest that PS synthesis is not the cause of septum ingression, although a complete three-layered septum with complete PS and SS will always be formed and will be essential for a safe cytokinesis and cell separation. Membrane trafficking and addition at the division site are key components of plant and fungal cytokinesis. Therefore, fungi have developed a particular cytokinesis (Fig. S8), sharing similarities (1) with animal cytokinesis, requiring a centripetal CR closure that in animal cells causes the plasma membrane deformation and constriction together with membrane addition until cell abscission; however, it cannot cause membrane deformation in the rigid cell wall–encased fungal cells; and (2) with plant cytokinesis, requiring membrane addition as an important mechanism to drive cytokinesis in walled cells (Fig. S8; Albertson et al., 2005; Prekeris and Gould, 2008; Müller and Jürgens, 2016; Smertenko et al., 2017).

Materials and methods
Strains and culture conditions
The *S. pombe* strains used in this study are listed in Table S1. The strains were made by genetic cross between the corresponding parental strains and either tetrads dissection or random spore selection against auxotrophies of both parental strains and analysis of the corresponding GFP or RFP localization.

GFP-12A-bgs1+ strains 1722 and 1723 were made as described for *GFP-bgs1+* strain 519 (Cortés et al., 2002) and contain an integrated copy of SmaI-cut pJK-*GFP-12A-bgs1+* (*leu1+* selection), which directs its integration at the SmaI site adjacent to *bgs1Δ::ura4+*, at position −748 of the *bgs1+* promoter sequence. *GFP-bgs1+* strain 1352 (*bgs1Δ*) is strain 519 (*bgs1Δ::ura4+*) made Ura⁻ by repeated growth in nonselective YES medium and selection of Ura⁻ colonies in minimal medium containing 5-fluoroorotic acid (5-FOA; 1 mg/ml). *GFP-12A-bgs1+* strain 1675 contains the selection marker *leu1+* adjacent to the *GFP-12A-bgs1+* sequence replacing the native *bgs1+* sequence. This strain was made from a Leu⁻ WT strain by homologous recombination of an ApaI-ApaI fragment of pSK-P*bgs1+*-*leu1+*-P*bgs1+*-*GFP-12A-bgs1(1-990)* (see below). Strains *tdTom-12A-bgs1+* 1780 and 3591 contain integrated SmaI-cut pJK-*tdTom-12A-bgs1+* (tandem dimer tdTomato variant of 2xRFP; Shaner et al., 2005) at position −748 of the *bgs1+* promoter sequence adjacent to *bgs1Δ::ura4+*. Strains with one to three tandem copies of the Cherry or one to two tandem copies of the Strawberry RFP variant containing a 12-alanine linker fused to Bgs1 were also tested. *Cher-12A-bgs1+* and *Str-12A-bgs1+* strains displayed lower RFP fluorescence and/or stability compared with that of *tdTom-12A-bgs1+*.

GFP-12A-bgs4+ strains 2364 and 2365 and *2xGFP-12A-bgs4+* strain 2285 contain integrated StuI-cut pJK-*GFP-12A-bgs4+* and pJK-*2xGFP-12A-bgs4+*, respectively, adjacent to *bgs4Δ::ura4+*, at position −1321 of the *bgs4+* promoter sequence. The obtained *GFP-12A-bgs1+*, *tdTom-12A-bgs1+*, *GFP-12A-bgs4+*, and *2xGFP-12A-bgs4+* strains displayed a WT phenotype and similar or improved GFP and RFP fluorescences and localizations with respect to those of previous fusions without the 12-alanine linker.

Strains *ags1+-12A-GFP-12A* 3166, 3167, 3168, and 3169 and *ags1+-8A-Cher-12A* strain 4004 have been described previously (Cortés et al., 2012) and contain integrated AgeI-cut pJK-*ags1(1-6267)-12A-GFP-12A* and pJK-*ags1(1-6267)-8A-Cher-12A*, respectively, at base 6025 of the *ags1+* coding sequence. These strains expressed functional Ags1-GFP and Ags1-RFP. Strains with two tandem copies of 8A-Cherry-12A or one to two tandem copies of 8A-tdTomato-12A were also tested. The *ags1+-8A-2xCher-12A* and *ags1+-8A-tdTom-12A* strains expressed a fully functional Ags1-RFP, whereas *ags1+-8A-2xtdTom-12A* only expressed a partially functional Ags1-RFP compared with that of *ags1+-8A-Cher-12A*. Ags1-GFP strains 3400 and 3402 are the strains 3167 and 3169,

Ramos et al.
Two septation phases discriminated by Bgs1 with LatA

Journal of Cell Biology
https://doi.org/10.1083/jcb.201808163

4189

respectively, made Ura⁻ by selection in minimal medium containing 5-FOA (1 mg/ml).

Pnmt1-81X-bgs1⁺ strain 1506 contains the selection marker ura4⁺ adjacent to the 81X version (low expression) of the thiamine-repressible nmt1⁺ promoter (Moreno et al., 2000), followed by the bgs1⁺ ORF. This strain was made from a Ura⁻ diploid strain by homologous recombination of an ApaI-NotI fragment of pSK-Pbgs1⁺-ura4⁺-81X-bgs1(1-983) (see below) and sporulation. The resulting 81X-bgs1⁺ haploid strain contained one single integrated bgs1⁺ copy under the control of the nmt1-81X promoter and exhibited a phenotype of elongated, branched, and multi-septated cells in the presence of thiamine (+T, repressed conditions) and a WT phenotype in its absence (–T, induced conditions) as described before (Cortés et al., 2007). The following 81X-bgs1⁺ strains 2076, 2078, and 2100 were made from strain 1506 by genetic cross and random spore analysis selecting against the corresponding parental auxotrophies. 81X-bgs1⁺ strain 2292 is strain 2078 made Ura⁻ by 5-FOA selection.

Strain bgs4Δ::ura4⁺ Pnmt1-81X-bgs4⁺ 1368 (his3⁺ selection) has been described previously (Muñoz et al., 2013) and contains the bgs4Δ::ura4⁺ deletion and one single integrated bgs4⁺ copy expressed under the control of the nmt1-81X promoter. Strain Pnmt1-81X-ags1⁺ 2086 has been described previously (Cortés et al., 2012) and contains one single integrated ags1⁺ copy expressed under the control of the nmt1-81X promoter. This strain was made from a Ura⁻ diploid strain by homologous recombination of an ApaI-ApaI fragment of pSK-Pags1⁺-ura4⁺-81X-ags1(1-2603) (see below) and sporulation. 81X-ags1⁺ strain 4373 was made from strain 2086 by genetic cross and random spore analysis selecting against the corresponding parental auxotrophies. The strains 81X-bgs4⁺ and 81X-ags1⁺ exhibit strong lytic phenotype in the presence of thiamine (+T, repressed conditions) and WT phenotype in its absence (–T, induced conditions).

Complete yeast growth (YES), selective (MM) with the appropriate supplements, and sporulation agar (SPA) media (Egel, 1984; Alfa et al., 1993) have been described previously. Selective MM+S is MM with 1.3 M sorbitol. Thiamine (+T; Sigma-Aldrich ref. T4625) was used at a 20-µg/ml final concentration (from a stock of 20 mg/ml in water). The actin-depolymerizing and monomer-sequestering drug LatA (Enzo Life Sciences) was used at a 100-µM final concentration (from a stock of 10 mM in DMSO). Under these conditions of high excess of LatA, all F-actin structures of cables, patches, and CR were depolymerized in <5 min as previously reported (Pelham and Chang, 2002; Wu et al., 2003; Proctor et al., 2012; Fujiwara et al., 2018). Cell growth was monitored by measuring the A_{600} of early log-phase cell populations in a SmartSpec 3000 spectrophotometer (Bio-Rad; A_{600} 0.1 = 10^6 cells/ml). The determinations were performed in two different clones of the same strain in two independent experiments.

Early log-phase cells were grown at 28°C in YES medium. The thermosensitive myosin myo2-E1 and formin cdc12-112 cells were grown at 25°C in YES+S medium and shifted to the restrictive temperatures of 28°C for 10–24 h, 32°C for 1–8 h, or 36°C for 1–8 h, as indicated in each case (see legends of Fig. 6 E and Fig. S5 B; Chang et al., 1997; Balasubramanian et al., 1998). Other

thermosensitive mutant cells (see legends of Fig. 8 C and Fig. S6 D) were grown at 25°C in YES medium, shifted to the corresponding highest permissive temperature and time before addition of LatA as specified, and kept at the same temperature during LatA treatment: septation initiation network (SIN) sid2-250 cells were shifted to 28°C for 2 h (highest limit before cell lysis initiation; Balasubramanian et al., 1998); rho1-596 cells were shifted to 32°C for 3 h (highest limit before cell lysis initiation; Viana et al., 2013); rgf3-1 (ehs2-1) and cdc42-L160S cells were shifted to 36°C for 4 h (highest limit before cell lysis initiation; Tajadura et al., 2004; Estravís et al., 2011); and sec8-1 cells were shifted to 32°C for 24 h before LatA treatment (highest permissive temperature; Wang et al., 2002). Constitutive cdc42-D76G mutant cells were grown and maintained at 28°C during LatA treatment (Estravís et al., 2011). 81X-bgs4⁺ and 81X-ags1⁺ cells were grown in MM at 28°C, transferred to YES+T (YES with additional 20 µg/ml thiamine) for 5 and 2 h, respectively (limit of cell lysis initiation during depletion of Bgs4 or Ags1), before LatA addition, and kept in the same medium during LatA treatment (Cortés et al., 2012; Muñoz et al., 2013). Similarly, 81X-bgs1⁺ cells were grown in MM at 28°C, transferred to YES+T for 5 h (initiation of the defect in septum degradation and cell separation during Bgs1 depletion) before LatA addition, and kept in the same medium during LatA treatment. Under these conditions, septum ingression without LatA of thermosensitive mutant cells, as well as 81X-bgs1⁺, 81X-bgs4⁺, and 81X-ags1⁺ mutant cells, proceeded similarly to that of the WT strain. The analysis of septa formed in the absence of Bgs1 was performed in 81X-bgs1⁺ cells grown in MM+S at 28°C and transferred to MM+S+T for 8, 10, 15, and 24 h, as described previously (Cortés et al., 2007). General procedures for yeast and bacterial culture and genetic manipulations were performed as described previously (Moreno et al., 1991; Sambrook and Russell, 2001).

Plasmids and DNA techniques

Plasmids pJK-bgs1⁺, pJK-bgs4⁺, and pJK-ags1(1-6267) have been described previously (Cortés et al., 2002, 2005, 2007, 2012). These plasmids are the integrative plasmid pJK148 (leu1⁺ selection) with an 8.8-kb ApaI-SpeI bgs1⁺, 8.8-kb PstI-NheI bgs4⁺, and 9.1-kb EcoRI-NheI ags1(1-6267) fragment, respectively.

A 12-alanine coding sequence used as a linker to provide flexibility was fused by site-directed mutagenesis (Kunkel, 1985) to the GFP 5′ and/or 3′-end coding sequence of pKS-GFP (Cortés et al., 2002), making pKS-GFP-12A, pKS-12A-GFP, and pKS-12A*-GFP-12A. 12A* indicates a nucleotide sequence different from 12A, thus avoiding homologous recombination. pKS-Cherry, pKS-Strawberry, and pKS-tdTomato are pKS⁺ with a BamHI-EcoRI fragment containing the 705-bp Cherry and Strawberry and 1,425-bp tdTomato coding sequences from pRSET-Cherry, pRSET-Strawberry, and pRSET-tdTomato variants of monomeric mRFP1, respectively (kindly provided by R. Tsien, University of California at San Diego, La Jolla, CA; Shaner et al., 2005). A 12-alanine coding sequence was fused to the RFP 3′-end coding sequence of pKS-Cherry, pKS-Strawberry, and pKS-tdTomato, making pKS-Cher-12A, pKS-Str-12A, and pKS-tdTom-12A, respectively. Similarly, 8- and 12-alanine coding sequences were fused

Ramos et al.
Two septation phases discriminated by Bgs1 with LatA

Journal of Cell Biology
https://doi.org/10.1083/jcb.201808163

4190

to the *Cherry* and *tdTomato* 5′ and 3′-end coding sequences, making pKS-*8A**-*Cher-12A* and pKS-*8A**-*tdTom-12A*, respectively.

pJK-*GFP-12A-bgs1*+, pJK-*GFP-12A-bgs4*+, and pJK-*2xGFP-12A-bgs4*+ are pJK-*bgs1*+ and pJK-*bgs4*+ with *GFP-12A* or tandem *2xGFP-12A* inserted in-frame after the start codon, at base 4 (amino acid 2) of *bgs1*+ and *bgs4*+ coding sequence, respectively. pJK-*tdTom-12A-bgs1*+ is pJK-*bgs1*+ with *tdTom-12A* inserted in-frame at base 4 of *bgs1*+ coding sequence. Similarly, pJK-*ags1(1-6267)-12A-GFP-12A* and pJK-*ags1(1-6267)-8A-Cher-12A* are pJK-*ags1(1-6267)* with *12A-GFP-12A* and *8A-Cher-12A*, respectively, inserted in-frame at base 5866 (amino acid 1956) of *ags1*+ coding sequence.

pSK-P*bgs1*+-*leu1*+-P*bgs1*+-*GFP-12A-bgs1(1-990)* contains a *bgs1*+ promoter fragment (nt −3029 to −2179), the *leu1*+ sequence (3.2 kb), and a P*bgs1*+-*GFP-12A-bgs1*+ 5′ ORF fragment (nt −2176 to +990) from pJK-*GFP-12A-bgs1*+. An ApaI-ApaI P*bgs1*+-*leu1*+-P*bgs1*+-*GFP-12A-bgs1(1-990)* fragment was used as a *bgs1*+ substitution cassette to make integrated *GFP-12A-bgs1*+ strains.

pSK-P*bgs1*+-*ura4*+-*81X-bgs1(1-983)* contains a *bgs1*+ promoter fragment (nt −2070 to −1088), the *ura4*+ sequence (2.2 kb), and a P*nmt1-81X-bgs1*+ 5′ ORF fragment (1.2 kb of *nmt1*+ promoter and nt +1 to +983 of *bgs1*+ 5′ ORF) from p81XL-*bgs1*+ (pJR102 version; Cortés et al., 2007). An ApaI-NotI P*bgs1*+-*ura4*+-*81X-bgs1(1-983)* fragment was used as a *bgs1*+ substitution cassette in a diploid strain to make integrated P*nmt1-81X-bgs1*+ strains.

p81XH-*bgs4*+ has been described previously (Cortés et al., 2005). This plasmid contains the *bgs4*+ ORF with XhoI and PstI sites inserted by site-directed mutagenesis just before the start codon and after the TAG stop codon of *bgs4*+, respectively, cloned into XhoI-PstI of pJR2-81XH (*his3*+ selection and *nmt1-81X* promoter; Moreno et al., 2000).

pSK-P*ags1*+-*ura4*+-*81X-ags1(1-2603)* has been described previously and contains an *ags1*+ promoter fragment (nt −2125 to −1099), the *ura4*+ sequence (2.2 kb), and a P*nmt1-81X-ags1*+ 5′ ORF fragment (1.2 kb of *nmt1*+ promoter and nt +1 to +2603 of *ags1*+ 5′ ORF) from p81XL-*ags1*+ (Cortés et al., 2012). An ApaI-ApaI P*ags1*+-*ura4*+-*81X-ags1(1-2603)* fragment was used as an *ags1*+ substitution cassette in a diploid strain to make integrated P*nmt1-81X-ags1*+ strains.

Microscopy techniques

For cell wall staining, early log-phase cells grown at 28°C in YES or YES + LatA (100 µM), with additional 20 µg/ml thiamine (+T) for cells repressing *bgs1*+, *bgs4*+, or *ags1*+, were concentrated (2,000 *g* for 30 s) and visualized directly by adding a solution of CW (50-µg/ml final concentration from a stock of 10 mg/ml in water [Blankophor, Bayer; Fluorescent Brightener 28, Sigma-Aldrich]) to the cell suspension and using the appropriate filter. GFP and RFP were visualized directly with the appropriate filters. Images were obtained with a fluorescence microscope (model DM RXA; Leica), a PL APO 63×/1.32 oil PH3 objective, a digital camera (model DFC350FX; Leica), and CW4000 cytoFISH software (Leica) and processed (brightness, contrast, and/or sharpness) with Adobe Photoshop CS2 software. All the analyses were repeated in three to seven independent experiments, and representative images of the analyzed phenotypes were interchangeably selected from the experiments. Graphical data were calculated from 3–20 independent experiments. The number of

experiments and of total septa or cells analyzed is shown in each case.

F-actin staining was performed as previously described (Marks and Hyams, 1985; Chang et al., 1996), with some changes. Early log-phase cells were fixed with 0.1 vol of PEM buffer (100 mM Pipes, 1 mM EGTA, and 1 mM MgSO$_4$, pH 6.9) and 0.2 vol of 16% ultra-pure EM-grade formaldehyde (Polysciences, ref. 18814) for 40–60 min at growth temperature. Cells were washed three times with PEM (2,000 *g* for 2 min), permeabilized with PEM + 1% Triton X-100 for 1 min, and washed three times with PEM. Cell pellets (1 µl) were incubated in 8 µl of Alexa Fluor 488–phalloidin (stored in MeOH in aliquots of 3 U/15 µl, dried, and reconstituted in 50 µl of PEM [Life Technologies, ref. A12379]) for 1 h at room temperature in the dark and stored at 4°C or visualized directly with the appropriate filter. Images were obtained with a fluorescence microscope (model DM RXA; Leica), a PL APO 63×/1.32 oil PH3 objective, a digital camera (model DFC350FX; Leica), and MetaMorph software (Molecular Devices). Maximal intensity projections of color images were created with ImageJ software (National Institutes of Health). Images in Fig. S1 B are maximal intensity projections of five Z-sections spaced at 0.30 µm. The analysis was repeated in three independent experiments, and representative images of the analyzed phenotypes were interchangeably selected from the experiments.

Time-lapse video imaging was performed essentially as previously described (Cortés et al., 2012). 0.5 ml of early log-phase cells grown in YES containing CW (5-µg/ml final concentration) at 28°C were collected by low-speed centrifugation (2,000 *g* for 30 s), resuspended in 300 µl of YES or YES + LatA medium containing CW (5-µg/ml final concentration), and placed in a well from a µ-Slide 8-well or a µ-Slide 8-well glass bottom (ibidi, ref. 80821-Uncoated and 80827) previously coated with 10 µl of 1-mg/ml soybean lectin (Sigma-Aldrich, ref. L1395). Time-lapse video experiments were made at 28°C by acquiring epifluorescence cell images in single planes and 1 × 1 binning on an inverted microscope (model IX71; Olympus) equipped with a PlanApo 100×/1.40 IX70 objective and a Personal DeltaVision system (Applied Precision). Images were captured using a CoolSnap HQ2 monochrome camera (Photometrics) and softWoRx 5.5.0 imaging software (Applied Precision) and restored by 3D Deconvolution (conservative ratio, 10 iterations, and high noise filtering) through softWoRx imaging software. Finally, images were processed (brightness and/or contrast) with ImageJ and Adobe Photoshop CS2 software. All the time-lapse videos were repeated, and the data were calculated from 3–30 independent experiments. The number of experiments and of total cells analyzed is shown in each case.

Measurements of septum length were made with the ImageJ software, using original images to avoid any artificial increase of fluorescence area and calibrating the measurement of images according to the used objective, 63× (1 pixel = 0.102 µm) or 100× (1 pixel = 0.0663 µm). Fluorescence intensity analysis of Bgs1 and CR proteins fused to RFP and GFP, respectively, was made with the integrated density function of ImageJ software and using original images acquired in the same conditions by placing a fixed circle on each fluorescent ring, measuring maximal and

Ramos et al.
Two septation phases discriminated by Bgs1 with LatA

Journal of Cell Biology 4191
https://doi.org/10.1083/jcb.201808163

total fluorescence values, and subtracting the background fluorescence value. Values are shown as arbitrary units (A.U.). Data distribution was assumed to be normal, but this was not formally tested.

TEM
Early log-phase cells grown in MM (100 ml), MM + 1.3 M sorbitol (100 ml), YES (100 ml), or YES + LatA (6 ml) at 28°C were collected and fixed with 2% glutaraldehyde EM (Electron Microscopy Science) in 50 mM phosphate buffer, pH 7.2, and 150 mM NaCl (PBS) for 2 h at 4°C, post-fixed with 1.2% potassium permanganate overnight at 4°C, and embedded in Quetol 812 as described previously (Konomi et al., 2003). Ultrathin sections were stained in 4% uranyl acetate and 0.4% lead citrate and viewed with a transmission electron microscope (Hitachi; model H-800) operating at 125 kV.

Online supplemental materials
Fig. S1 shows that the septum of cells growing in the absence of F-actin is able to ingress to completion and that the percentage of cells with septa decreases along the time of LatA treatment. Fig. S2 shows that the complete septa formed in cells deprived of F-actin can be degraded for cell separation. Fig. S3 shows that cells deprived of F-actin exhibit three different septum stages depending on the phase of septum ingression and on the type of Bgs1 glucan synthase localization to the septum membrane. Fig. S4 shows that the formation of thick septa, which is triggered by the loss of the landmark function of the CR, ultimately depends on the Bgs1 ring loss. Fig. S5 shows that Bgs1 depletion originates thick septa that do not depend on the loss of CR proteins, whose localization is not affected, but on the ensuing loss of Ags1 and Bgs4 rings. Fig. S6 shows that the ingression of stable mature septa (phase 2 septa) in cells deprived of F-actin is controlled by glucan synthase and Rho regulatory proteins. Fig. S7 shows that the sharp septum edges can be classified into three types according to a gradual increase in the sharp-edge phenotype. Fig. S8 shows that fungal cytokinesis shares similarities with animal and plant cytokinesis and shows models of animal, plant, and fungal cytokinesis. Video 1 is a time-lapse video of a representative field of WT cells showing the two phases of septum ingression with different levels of CW staining. Table S1 lists the fission yeast strains used in this study.

Acknowledgements

References

Albertson, R., B. Riggs, and W. Sullivan. 2005. Membrane traffic: a driving force in cytokinesis. *Trends Cell Biol.* 15:92–101. https://doi.org/10.1016/j.tcb.2004.12.008

Alfa, C., P. Fantes, J. Hyams, M. McLeod, and E. Warbrick. 1993. *Experiments with Fission Yeast: A Laboratory Course Manual.* Cold Spring Harbor Laboratory Press, Cold Spring Harbor, NY. 186 pp.

Arai, R., K. Nakano, and I. Mabuchi. 1998. Subcellular localization and possible function of actin, tropomyosin and actin-related protein 3 (Arp3) in the fission yeast *Schizosaccharomyces pombe*. *Eur. J. Cell Biol.* 76: 288–295. https://doi.org/10.1016/S0171-9335(98)80007-1

Arasada, R., and T.D. Pollard. 2014. Contractile ring stability in *S. pombe* depends on F-BAR protein Cdc15p and Bgs1p transport from the Golgi complex. *Cell Reports.* 8:1533–1544. https://doi.org/10.1016/j.celrep.2014.07.048

Atkins, B.D., S. Yoshida, K. Saito, C.F. Wu, D.J. Lew, and D. Pellman. 2013. Inhibition of Cdc42 during mitotic exit is required for cytokinesis. *J. Cell Biol.* 202:231–240. https://doi.org/10.1083/jcb.201301090

Balasubramanian, M.K., D. McCollum, L. Chang, K.C. Wong, N.I. Naqvi, X. He, S. Sazer, and K.L. Gould. 1998. Isolation and characterization of new fission yeast cytokinesis mutants. *Genetics.* 149:1265–1275.

Barnett, J.A., and C.F. Robinow. 2002. A history of research on yeasts 4: cytology part II, 1950-1990. *Yeast.* 19:745–772. https://doi.org/10.1002/yea.875

Bhavsar-Jog, Y.P., and E. Bi. 2017. Mechanics and regulation of cytokinesis in budding yeast. *Semin. Cell Dev. Biol.* 66:107–118. https://doi.org/10.1016/j.semcdb.2016.12.010

Cabib, E., and J. Arroyo. 2013. How carbohydrates sculpt cells: chemical control of morphogenesis in the yeast cell wall. *Nat. Rev. Microbiol.* 11: 648–655. https://doi.org/10.1038/nrmicro3090

Calonge, T.M., K. Nakano, M. Arellano, R. Arai, S. Katayama, T. Toda, I. Mabuchi, and P. Pérez. 2000. *Schizosaccharomyces pombe* rho2p GTPase regulates cell wall α-glucan biosynthesis through the protein kinase pck2p. *Mol. Biol. Cell.* 11:4393–4401. https://doi.org/10.1091/mbc.11.12.4393

Chang, F., A. Woollard, and P. Nurse. 1996. Isolation and characterization of fission yeast mutants defective in the assembly and placement of the contractile actin ring. *J. Cell Sci.* 109:131–142.

Chang, F., D. Drubin, and P. Nurse. 1997. cdc12p, a protein required for cytokinesis in fission yeast, is a component of the cell division ring and

interacts with profilin. *J. Cell Biol.* 137:169–182. https://doi.org/10.1083/jcb.137.1.169

Cheffings, T.H., N.J. Burroughs, and M.K. Balasubramanian. 2016. Actomyosin ring formation and tension generation in eukaryotic cytokinesis. *Curr. Biol.* 26:R719–R737. https://doi.org/10.1016/j.cub.2016.06.071

Coll, P.M., S.A. Rincón, R.A. Izquierdo, and P. Pérez. 2007. Hob3p, the fission yeast ortholog of human BIN3, localizes Cdc42p to the division site and regulates cytokinesis. *EMBO J.* 26:1865–1877. https://doi.org/10.1038/sj.emboj.7601641

Cortés, J.C.G., J. Ishiguro, A. Durán, and J.C. Ribas. 2002. Localization of the (1,3)β-D-glucan synthase catalytic subunit homologue Bgs1p/Cps1p from fission yeast suggests that it is involved in septation, polarized growth, mating, spore wall formation and spore germination. *J. Cell Sci.* 115:4081–4096. https://doi.org/10.1242/jcs.00085

Cortés, J.C.G., E. Carnero, J. Ishiguro, Y. Sánchez, A. Durán, and J.C. Ribas. 2005. The novel fission yeast (1,3)β-D-glucan synthase catalytic subunit Bgs4p is essential during both cytokinesis and polarized growth. *J. Cell Sci.* 118:157–174. https://doi.org/10.1242/jcs.01585

Cortés, J.C.G., M. Konomi, I.M. Martins, J. Muñoz, M.B. Moreno, M. Osumi, A. Durán, and J.C. Ribas. 2007. The (1,3)β-D-glucan synthase subunit Bgs1p is responsible for the fission yeast primary septum formation. *Mol. Microbiol.* 65:201–217. https://doi.org/10.1111/j.1365-2958.2007.05784.x

Cortés, J.C.G., M. Sato, J. Muñoz, M.B. Moreno, J.A. Clemente-Ramos, M. Ramos, H. Okada, M. Osumi, A. Durán, and J.C. Ribas. 2012. Fission yeast Ags1 confers the essential septum strength needed for safe gradual cell abscission. *J. Cell Biol.* 198:637–656. https://doi.org/10.1083/jcb.201202015

Cortés, J.C.G., N. Pujol, M. Sato, M. Pinar, M. Ramos, B. Moreno, M. Osumi, J.C. Ribas, and P. Pérez. 2015. Cooperation between paxillin-like protein Pxl1 and glucan synthase Bgs1 is essential for actomyosin ring stability and septum formation in fission yeast. *PLoS Genet.* 11:e1005358. https://doi.org/10.1371/journal.pgen.1005358

Cortés, J.C.G., M. Ramos, M. Konomi, I. Barragán, M.B. Moreno, M. Alcaide-Gavilán, S. Moreno, M. Osumi, P. Pérez, and J.C. Ribas. 2018. Specific detection of fission yeast primary septum reveals septum and cleavage furrow ingression during early anaphase independent of mitosis completion. *PLoS Genet.* 14:e1007388. https://doi.org/10.1371/journal.pgen.1007388

Davidson, R., J.A. Pontasch, and J.Q. Wu. 2016. Sbg1 is a novel regulator for the localization of the β-glucan synthase Bgs1 in fission yeast. *PLoS One.* 11:e0167043. https://doi.org/10.1371/journal.pone.0167043

Donoso, I., M.C. Muñoz-Centeno, M.A. Sànchez-Durán, A. Flores, R.R. Daga, C.M. Guevara, and E.R. Bejarano. 2005. Mpg1, a fission yeast protein required for proper septum structure, is involved in cell cycle progression through cell-size checkpoint. *Mol. Genet. Genomics.* 274:155–167. https://doi.org/10.1007/s00438-005-0005-8

Egel, R. 1984. Two tightly linked silent cassettes in the mating-type region of *Schizosaccharomyces pombe. Curr. Genet.* 8:199–203. https://doi.org/10.1007/BF00417816

Eggert, U.S., T.J. Mitchison, and C.M. Field. 2006. Animal cytokinesis: from parts list to mechanisms. *Annu. Rev. Biochem.* 75:543–566. https://doi.org/10.1146/annurev.biochem.74.082803.133425

Estravís, M., S.A. Rincón, B. Santos, and P. Pérez. 2011. Cdc42 regulates multiple membrane traffic events in fission yeast. *Traffic.* 12:1744–1758. https://doi.org/10.1111/j.1600-0854.2011.01275.x

Figard, L., H. Xu, H.G. Garcia, I. Golding, and A.M. Sokac. 2013. The plasma membrane flattens out to fuel cell-surface growth during *Drosophila* cellularization. *Dev. Cell.* 27:648–655. https://doi.org/10.1016/j.devcel.2013.11.006

Free, S.J. 2013. Fungal cell wall organization and biosynthesis. *Adv. Genet.* 81:33–82. https://doi.org/10.1016/B978-0-12-407677-8.00002-6

Fujiwara, I., M.E. Zweifel, N. Courtemanche, and T.D. Pollard. 2018. Latrunculin A accelerates actin filament depolymerization in addition to sequestering actin monomers. *Curr. Biol.* 28:3183–3192. https://doi.org/10.1016/B978-0-12-407677-8.00002-6

García, P., V. Tajadura, I. García, and Y. Sánchez. 2006. Rgf1p is a specific Rho1-GEF that coordinates cell polarization with cell wall biogenesis in fission yeast. *Mol. Biol. Cell.* 17:1620–1631. https://doi.org/10.1091/mbc.e05-10-0933

García Cortés, J.C., M. Ramos, M. Osumi, P. Pérez, and J.C. Ribas. 2016. The cell biology of fission yeast septation. *Microbiol. Mol. Biol. Rev.* 80:779–791. https://doi.org/10.1128/MMBR.00013-16

Glotzer, M. 2017. Cytokinesis in metazoa and fungi. *Cold Spring Harb. Perspect. Biol.* 9:a022343. https://doi.org/10.1101/cshperspect.a022343

Gow, N.A.R., J.P. Latge, and C.A. Munro. 2017. The fungal cell wall: structure, biosynthesis, and function. *Microbiol. Spectr.* 5. https://doi.org/10.1128/microbiolspec.FUNK-0035-2016

Green, R.A., E. Paluch, and K. Oegema. 2012. Cytokinesis in animal cells. *Annu. Rev. Cell Dev. Biol.* 28:29–58. https://doi.org/10.1146/annurev-cellbio-101011-155718

Heider, M.R., and M. Munson. 2012. Exorcising the exocyst complex. *Traffic.* 13:898–907. https://doi.org/10.1111/j.1600-0854.2012.01353.x

Hochstenbach, F., F.M. Klis, H. van den Ende, E. van Donselaar, P.J. Peters, and R.D. Klausner. 1998. Identification of a putative α-glucan synthase essential for cell wall construction and morphogenesis in fission yeast. *Proc. Natl. Acad. Sci. USA.* 95:9161–9166. https://doi.org/10.1073/pnas.95.16.9161

Humbel, B.M., M. Konomi, T. Takagi, N. Kamasawa, S.A. Ishijima, and M. Osumi. 2001. In situ localization of β-glucans in the cell wall of *Schizosaccharomyces pombe. Yeast.* 18:433–444. https://doi.org/10.1002/yea.694

Johnson, B.F., B.Y. Yoo, and G.B. Calleja. 1973. Cell division in yeasts: movement of organelles associated with cell plate growth of *Schizosaccharomyces pombe. J. Bacteriol.* 115:358–366.

Johnson, B.F., B.Y. Yoo, G.B. Calleja, and C.P. Kozela. 2005. Second thoughts on septation by the fission yeast, *Schizosaccharomyces pombe*: pull vs. push mechanisms with an appendix--dimensional modelling of the flat and variable septa. *Antonie van Leeuwenhoek.* 88:1–12. https://doi.org/10.1007/s10482-004-7074-2

Jourdain, I., H.C. Dooley, and T. Toda. 2012. Fission yeast sec3 bridges the exocyst complex to the actin cytoskeleton. *Traffic.* 13:1481–1495. https://doi.org/10.1111/j.1600-0854.2012.01408.x

Juanes, M.A., and S. Piatti. 2016. The final cut: cell polarity meets cytokinesis at the bud neck in *S. cerevisiae. Cell. Mol. Life Sci.* 73:3115–3136. https://doi.org/10.1007/s00018-016-2220-3

Kanbe, T., I. Kobayashi, and K. Tanaka. 1989. Dynamics of cytoplasmic organelles in the cell cycle of the fission yeast *Schizosaccharomyces pombe*: three-dimensional reconstruction from serial sections. *J. Cell Sci.* 94:647–656.

Kanbe, T., T. Akashi, and K. Tanaka. 1993. Effect of cytochalasin A on actin distribution in the fission yeast *Schizosaccharomyces pombe* studied by fluorescent and electron microscopy. *Protoplasma.* 176:24–32. https://doi.org/10.1007/BF01378936

Katayama, S., D. Hirata, M. Arellano, P. Pérez, and T. Toda. 1999. Fission yeast α-glucan synthase Mok1 requires the actin cytoskeleton to localize the sites of growth and plays an essential role in cell morphogenesis downstream of protein kinase C function. *J. Cell Biol.* 144:1173–1186. https://doi.org/10.1083/jcb.144.6.1173

Konomi, M., K. Fujimoto, T. Toda, and M. Osumi. 2003. Characterization and behaviour of α-glucan synthase in *Schizosaccharomyces pombe* as revealed by electron microscopy. *Yeast.* 20:427–438. https://doi.org/10.1002/yea.974

Kovar, D.R., V. Sirotkin, and M. Lord. 2011. Three's company: the fission yeast actin cytoskeleton. *Trends Cell Biol.* 21:177–187. https://doi.org/10.1016/j.tcb.2010.11.001

Kunkel, T.A. 1985. Rapid and efficient site-specific mutagenesis without phenotypic selection. *Proc. Natl. Acad. Sci. USA.* 82:488–492. https://doi.org/10.1073/pnas.82.2.488

Liu, J., X. Tang, H. Wang, S. Oliferenko, and M.K. Balasubramanian. 2002. The localization of the integral membrane protein Cps1p to the cell division site is dependent on the actomyosin ring and the septation-inducing network in *Schizosaccharomyces pombe. Mol. Biol. Cell.* 13:989–1000. https://doi.org/10.1091/mbc.01-12-0581

Maeda, Y., J. Kashiwazaki, C. Shimoda, and T. Nakamura. 2009. The *Schizosaccharomyces pombe* syntaxin 1 homolog, Psy1, is essential in the development of the forespore membrane. *Biosci. Biotechnol. Biochem.* 73:339–345. https://doi.org/10.1271/bbb.80575

Marks, J., and J.S. Hyams. 1985. Localization of F-actin through the cell division cycle of *Schizosaccharomyces pombe. Eur. J. Cell Biol.* 39:27–32.

Martín-García, R., V. Arribas, P.M. Coll, M. Pinar, R.A. Viana, S.A. Rincón, J. Correa-Bordes, J.C. Ribas, and P. Pérez. 2018. Paxillin-mediated recruitment of calcineurin to the contractile ring is required for the correct progression of cytokinesis in fission yeast. *Cell Rep.* 25:772-783.

Martins, I.M., J.C.G. Cortés, J. Muñoz, M.B. Moreno, M. Ramos, J.A. Clemente-Ramos, A. Durán, and J.C. Ribas. 2011. Differential activities of three families of specific β(1,3)glucan synthase inhibitors in wild-type and resistant strains of fission yeast. *J. Biol. Chem.* 286:3484–3496. https://doi.org/10.1074/jbc.M110.174300

Mateos, P., and A. Domínguez. 1991. Ultrastructure and cell wall composition in cell division cycle mutants of *Schizosaccharomyces pombe* deficient in septum formation. *Antonie van Leeuwenhoek.* 59:155–165.

Moreno, M.B., A. Durán, and J.C. Ribas. 2000. A family of multifunctional thiamine-repressible expression vectors for fission yeast. *Yeast.* 16:

861–872. https://doi.org/10.1002/1097-0061(20000630)16:9<861::AID-YEA577>3.0.CO;2-9

Moreno, S., A. Klar, and P. Nurse. 1991. Molecular genetic analysis of fission yeast *Schizosaccharomyces pombe*. *Methods Enzymol.* 194:795–823. https://doi.org/10.1016/0076-6879(91)94059-L

Mouyna, I., L. Hartl, and J.P. Latgé. 2013. β-1,3-glucan modifying enzymes in *Aspergillus fumigatus*. *Front. Microbiol.* 4:81. https://doi.org/10.3389/fmicb.2013.00081

Müller, S., and G. Jürgens. 2016. Plant cytokinesis-No ring, no constriction but centrifugal construction of the partitioning membrane. *Semin. Cell Dev. Biol.* 53:10–18. https://doi.org/10.1016/j.semcdb.2015.10.037

Mulvihill, D.P., S.R. Edwards, and J.S. Hyams. 2006. A critical role for the type V myosin, Myo52, in septum deposition and cell fission during cytokinesis in *Schizosaccharomyces pombe*. *Cell Motil. Cytoskeleton*. 63:149–161. https://doi.org/10.1002/cm.20113

Muñoz, J., J.C. Cortés, M. Sipiczki, M. Ramos, J.A. Clemente-Ramos, M.B. Moreno, I.M. Martins, P. Pérez, and J.C. Ribas. 2013. Extracellular cell wall β(1,3)glucan is required to couple septation to actomyosin ring contraction. *J. Cell Biol.* 203:265–282. https://doi.org/10.1083/jcb.201304132

Nakano, K., T. Mutoh, R. Arai, and I. Mabuchi. 2003. The small GTPase Rho4 is involved in controlling cell morphology and septation in fission yeast. *Genes Cells.* 8:357–370. https://doi.org/10.1046/j.1365-2443.2003.00639.x

Naqvi, N.I., K. Eng, K.L. Gould, and M.K. Balasubramanian. 1999. Evidence for F-actin-dependent and -independent mechanisms involved in assembly and stability of the medial actomyosin ring in fission yeast. *EMBO J.* 18:854–862. https://doi.org/10.1093/emboj/18.4.854

Oberti, D., A. Biasini, M.A. Kirschmann, C. Genoud, R. Stunnenberg, Y. Shimada, and M. Bühler. 2015. Dicer and Hsp104 function in a negative feedback loop to confer robustness to environmental stress. *Cell Reports.* 10:47–61. https://doi.org/10.1016/j.celrep.2014.12.006

Onishi, M., N. Ko, R. Nishihama, and J.R. Pringle. 2013. Distinct roles of Rho1, Cdc42, and Cyk3 in septum formation and abscission during yeast cytokinesis. *J. Cell Biol.* 202:311–329. https://doi.org/10.1083/jcb.201302001

Osumi, M. 2012. Visualization of yeast cells by electron microscopy. *J. Electron Microsc. (Tokyo).* 61:343–365. https://doi.org/10.1093/jmicro/dfs082

Osumi, M., M. Konomi, T. Sugawara, T. Takagi, and M. Baba. 2006. High-pressure freezing is a powerful tool for visualization of *Schizosaccharomyces pombe* cells: ultra-low temperature and low-voltage scanning electron microscopy and immunoelectron microscopy. *J. Electron Microsc. (Tokyo).* 55:75–88. https://doi.org/10.1093/jmicro/dfl014

Pelham, R.J., and F. Chang. 2002. Actin dynamics in the contractile ring during cytokinesis in fission yeast. *Nature.* 419:82–86. https://doi.org/10.1038/nature00999

Pérez, P., and S.A. Rincón. 2010. Rho GTPases: regulation of cell polarity and growth in yeasts. *Biochem. J.* 426:243–253. https://doi.org/10.1042/BJ20091823

Pérez, P., J.C.G. Cortés, R. Martín-García, and J.C. Ribas. 2016. Overview of fission yeast septation. *Cell. Microbiol.* 18:1201–1207. https://doi.org/10.1111/cmi.12611

Pollard, T.D. 2017. Nine unanswered questions about cytokinesis. *J. Cell Biol.* 216:3007–3016. https://doi.org/10.1083/jcb.201612068

Pollard, T.D., and J.Q. Wu. 2010. Understanding cytokinesis: lessons from fission yeast. *Nat. Rev. Mol. Cell Biol.* 11:149–155. https://doi.org/10.1038/nrm2834

Pollard, L.W., M. Onishi, J.R. Pringle, and M. Lord. 2012. Fission yeast Cyk3p is a transglutaminase-like protein that participates in cytokinesis and cell morphogenesis. *Mol. Biol. Cell.* 23:2433–2444. https://doi.org/10.1091/mbc.e11-07-0656

Prekeris, R., and G.W. Gould. 2008. Breaking up is hard to do - membrane traffic in cytokinesis. *J. Cell Sci.* 121:1569–1576. https://doi.org/10.1242/jcs.018770

Proctor, S.A., N. Minc, A. Boudaoud, and F. Chang. 2012. Contributions of turgor pressure, the contractile ring, and septum assembly to forces in cytokinesis in fission yeast. *Curr. Biol.* 22:1601–1608. https://doi.org/10.1016/j.cub.2012.06.042

Royou, A., C. Field, J.C. Sisson, W. Sullivan, and R. Karess. 2004. Reassessing the role and dynamics of nonmuscle myosin II during furrow formation in early *Drosophila* embryos. *Mol. Biol. Cell.* 15:838–850. https://doi.org/10.1091/mbc.e03-06-0440

Sambrook, J., and D.W. Russell. 2001. *Molecular Cloning: A Laboratory Manual.* Cold Spring Harbor Laboratory Press, Cold Spring Harbor, NY. 2344 pp.

Sethi, K., S. Palani, J.C. Cortés, M. Sato, M. Sevugan, M. Ramos, S. Vijaykumar, M. Osumi, N.I. Naqvi, J.C. Ribas, and M. Balasubramanian. 2016. A new membrane protein Sbg1 links the contractile ring apparatus and septum synthesis machinery in fission yeast. *PLoS Genet.* 12:e1006383. https://doi.org/10.1371/journal.pgen.1006383

Shaner, N.C., P.A. Steinbach, and R.Y. Tsien. 2005. A guide to choosing fluorescent proteins. *Nat. Methods.* 2:905–909. https://doi.org/10.1038/nmeth819

Sipiczki, M. 2016. Visualization of fission yeast cells by transmission electron microscopy. *Methods Mol. Biol.* 1369:97–111. https://doi.org/10.1007/978-1-4939-3145-3_8

Smertenko, A., F. Assaad, F. Baluška, M. Bezanilla, H. Buschmann, G. Drakakaki, M.T. Hauser, M. Janson, Y. Mineyuki, I. Moore, et al. 2017. Plant cytokinesis: terminology for structures and processes. *Trends Cell Biol.* 27:885–894. https://doi.org/10.1016/j.tcb.2017.08.008

Stachowiak, M.R., C. Laplante, H.F. Chin, B. Guirao, E. Karatekin, T.D. Pollard, and B. O'Shaughnessy. 2014. Mechanism of cytokinetic contractile ring constriction in fission yeast. *Dev. Cell.* 29:547–561. https://doi.org/10.1016/j.devcel.2014.04.021

Tajadura, V., B. García, I. García, P. García, and Y. Sánchez. 2004. *Schizosaccharomyces pombe* Rgf3p is a specific Rho1 GEF that regulates cell wall β-glucan biosynthesis through the GTPase Rho1p. *J. Cell Sci.* 117:6163–6174. https://doi.org/10.1242/jcs.01530

Thiyagarajan, S., E.L. Munteanu, R. Arasada, T.D. Pollard, and B. O'Shaughnessy. 2015. The fission yeast cytokinetic contractile ring regulates septum shape and closure. *J. Cell Sci.* 128:3672–3681. https://doi.org/10.1242/jcs.166926

Viana, R.A., M. Pinar, T. Soto, P.M. Coll, J. Cansado, and P. Pérez. 2013. Negative functional interaction between cell integrity MAPK pathway and Rho1 GTPase in fission yeast. *Genetics.* 195:421–432. https://doi.org/10.1534/genetics.113.154807

Vjestica, A., X.Z. Tang, and S. Oliferenko. 2008. The actomyosin ring recruits early secretory compartments to the division site in fission yeast. *Mol. Biol. Cell.* 19:1125–1138. https://doi.org/10.1091/mbc.e07-07-0663

Wang, Y.L. 2005. The mechanism of cortical ingression during early cytokinesis: thinking beyond the contractile ring hypothesis. *Trends Cell Biol.* 15:581–588. https://doi.org/10.1016/j.tcb.2005.09.006

Wang, H., X. Tang, J. Liu, S. Trautmann, D. Balasundaram, D. McCollum, and M.K. Balasubramanian. 2002. The multiprotein exocyst complex is essential for cell separation in *Schizosaccharomyces pombe*. *Mol. Biol. Cell.* 13:515–529. https://doi.org/10.1091/mbc.01-11-0542

Wang, N., I.J. Lee, G. Rask, and J.Q. Wu. 2016. Roles of the TRAPP-II complex and the exocyst in membrane deposition during fission yeast cytokinesis. *PLoS Biol.* 14:e1002437. https://doi.org/10.1371/journal.pbio.1002437

Wei, B., B.S. Hercyk, N. Mattson, A. Mohammadi, J. Rich, E. DeBruyne, M.M. Clark, and M. Das. 2016. Unique spatiotemporal activation pattern of Cdc42 by Gef1 and Scd1 promotes different events during cytokinesis. *Mol. Biol. Cell.* 27:1235–1245. https://doi.org/10.1091/mbc.E15-10-0700

Wu, J.Q., J.R. Kuhn, D.R. Kovar, and T.D. Pollard. 2003. Spatial and temporal pathway for assembly and constriction of the contractile ring in fission yeast cytokinesis. *Dev. Cell.* 5:723–734. https://doi.org/10.1016/S1534-5807(03)00324-1

Zhou, Z., E.L. Munteanu, J. He, T. Ursell, M. Bathe, K.C. Huang, and F. Chang. 2015. The contractile ring coordinates curvature-dependent septum assembly during fission yeast cytokinesis. *Mol. Biol. Cell.* 26:78–90. https://doi.org/10.1091/mbc.e14-10-1441

Zhu, Y.H., J. Hyun, Y.Z. Pan, J.E. Hopper, J. Rizo, and J.Q. Wu. 2018. Roles of the fission yeast UNC-13/Munc13 protein Ync13 in late stages of cytokinesis. *Mol. Biol. Cell.* 29:2259–2279. https://doi.org/10.1091/mbc.E18-04-0225